THESIS

# USE OF GLOBAL DATASETS FOR DOWNSCALING SOIL MOISTURE WITH THE EMT+VS MODEL

Submitted by

Nicholas R. Grieco

Department of Civil and Environmental Engineering

In partial fulfillment of the requirements

For the Degree of Master of Science

Colorado State University

Fort Collins, Colorado

Fall 2017

Master's Committee:

Advisor: Jeffrey D. Niemann

Timothy R. Green
Gregory L. Butters

ABSTRACT

USE OF GLOBAL DATASETS FOR DOWNSCALING SOIL MOISTURE WITH THE EMT+VS MODEL

Satellite remote sensing and land-surface models provide coarse-resolution (9-40 km) soil moisture estimates, but various applications require fine-resolution (10-30 m) soil moisture patterns. The Equilibrium Moisture from Topography, Vegetation, and Soil (EMT+VS) model downscales soil moisture using fine-resolution topography, vegetation, and soil data. It has been shown to reproduce temporally unstable soil moisture patterns (i.e. patterns where the spatial structure varies in time). It can also reproduce hillslope dependent patterns (wetter locations occur on hillslopes oriented away from the sun) and valley dependent patterns (wetter locations occur in valley bottoms). However, the EMT+VS model requires several parameters to characterize the local climate, soil, and vegetation characteristics. In previous applications, the parameters were calibrated using point soil moisture data, but many regions of interest may not have such data. The purpose of this study is to evaluate EMT+VS model performance when the parameters are estimated from global datasets without site-specific calibration. Reliable and accessible global datasets were identified and methods were developed to estimate the parameters from the datasets. The global model (without site-specific calibration) was applied to six study sites, and its results were compared to local soil moisture observations and the results from the locally calibrated model. The use of global datasets decreased downscaling performance and the spatial variability of soil moisture was underestimated. Overall, only 5 of the 16 parameters can be estimated from global datasets. However, the global model still

provides more reliable soil moisture estimates than the coarse-resolution input for most sampling dates at all six study sites.

# ACKNOWLEDGEMENTS

Financial support from the Army Research Lab (ARL) Small Business Innovative Research (SBIR) program is gratefully acknowledged.

TABLE OF CONTENTS

ABSTRACT ..... ii

ACKNOWLEDGEMENTS ..... iv

1. INTRODUCTION ..... 1

2. EMT+VS MODEL AND PARAMETERS ..... 6

3. APPLICATION TO STUDY SITES ..... 11

3.1 STUDY SITES ..... 11

3.2 MODEL APPLICATION ..... 13

4. REFERENCE PARAMETER VALUES ..... 16

4.1 CLIMATE PARAMETERS ..... 16

4.2 SOIL PARAMETERS ..... 18

4.3 VEGETATION PARAMETERS ..... 20

5. EVALUATING REFERENCE PARAMETERS ..... 23

6. RECOMMENDED PARAMETERS ..... 28

7. GLOBAL MODEL PERFORMANCE ..... 31

8. CONCLUSIONS ..... 36

TABLES AND FIGURES ..... 39

REFERENCES ..... 49

APPENDIX ..... 57

LIST OF ABBREVIATIONS ..... 58

# 1. INTRODUCTION

Fine-resolution (10-30 m) patterns of volumetric water content (soil moisture) over watershed scales are important for modeling land-atmosphere interactions (Delworth and Manabe, 1989), hydrologic response (Houser et al., 1998), weather patterns (Seuffert et al., 2002), and climate behavior (Dirmeyer, 1999). They are also beneficial for practical applications such as drought monitoring (Bolten et al., 2010), wildfire prediction (Nelson, 2001), agricultural production (Green and Erskine, 2004; Yuge et al., 2016), soil mechanics (Flores et al., 2014; Horn and Fleige, 2003; Vero et al., 2014), and soil erosion (Singh and Thompson, 2016).

Coarse-resolution soil moisture can be estimated from satellite remote sensing. Passive microwave radiometers such as Advanced Microwave Scanning Radiometer (AMSR-E) (see List of Abbreviations) (Njoku et al., 2003), AMSR2 (Parinussa et al., 2015), and WindSat (Li et al., 2010) measure radiation at various frequencies, providing frequent soil moisture estimates (0.5-2 days) but at coarse resolutions (5-60 km). More recently, synthetic aperture radiometers like Soil Moisture Ocean Salinity (SMOS) incorporated the L-band (Kerr et al., 2010) to improve soil moisture estimation. Soil Moisture Active and Passive (SMAP) was designed to use both active microwave radiometry and passive L-band observations (Entekhabi et al., 2010). This approach can provide moderate resolution (9 km) soil moisture estimates but is affected by vegetation (Das et al., 2014). The Advanced Scatterometer (ASCAT) uses a real-aperture radar instrument to measure surface radar backscatter and estimate soil moisture (Bartalis et al., 2007).

Coarse-resolution soil moisture can also be provided by land-surface models. These models simulate various physical, biological, and chemical processes that affect soil moisture, and they vary in their specific inputs and outputs (Williams et al., 2009). Some examples are

Noah (Kumar et al., 2014), Variable Infiltration Capacity (VIC) (Liang et al., 1996), Mosaic (Koster and Suarez, 2003), simple biosphere (SiB) (Sellers et al., 1986), TOPMODEL-Based Land-Atmosphere Transfer Scheme (TOPLATS) (Famiglietti and Wood, 1994), Community Land Model (CLM) (Bonan, 1998), and European Centre for Medium-Range Weather Forecasts (ECMWF) (Viterbo and Beljaars, 1995).

To reach the spatial resolutions required by the applications listed earlier, such coarse-resolution data must be downscaled. Available downscaling methods can be grouped by the supplemental data they use (satellites, statistical models, land-surface models, or geo-information) (Peng et al., 2017). Many satellite-based methods use optical/thermal data to determine a downscaling factor for the improvement of fine-resolution soil moisture variability (Carlson, 2007; Chauhan et al., 2003; Kim and Hogue, 2012; Merlin et al., 2013; Piles et al., 2016). Statistical downscaling methods maintain the statistics of *in situ* and/or fine-resolution remotely sensed soil moisture observations across or within scales (Kaheil et al., 2008; Kim and Barros, 2002; Mascaro et al., 2010; Perry and Niemann, 2007). Land-surface models can be used for downscaling by applying the model regionally at a fine-resolution and adjusting model parameters so that the model's coarse-resolution soil moisture matches the known value (Ines et al., 2013). Remotely sensed data can be assimilated for downscaling with land-surface models (Sahoo et al., 2013). Land-surface models are also useful for reproducing the statistical properties of fine-resolution soil moisture (Verhoest et al., 2015). Geo-information methods infer fine-resolution soil moisture variations from relationships to topographic, vegetation, and/or soil characteristics (Busch et al., 2012; Droesen, 2016; Pellenq et al., 2003; Temimi et al., 2010; Werbylo and Niemann, 2014; Wilson et al., 2005).

The Equilibrium Moisture from Topography, Vegetation, and Soil (EMT+VS) model was classified by Peng et al. (2017) as a geo-information method. It models the water balance of the vadose zone and infers spatial variations in the relevant hydrologic processes from topographic, vegetation, and soil information. It was first applied to small catchments using only fine-resolution topographic data, and its results were compared to gridded *in situ* soil moisture observations. It was shown to reproduce both hillslope and valley dependent soil moisture patterns as well as temporal instability (Coleman and Niemann, 2013). It was later generalized to accept fine-resolution vegetation and soil data if available (Ranney et al., 2015). The model was further extended to apply to regions with large topographic relief (Cowley et al., 2017) and regions that span multiple coarse grid cells (Hoehn et al., 2017).

In all previous testing, the EMT+VS model parameters were calibrated using point observations of soil moisture. Ranges for calibrated parameters were constrained using local information about the physical characteristics (Cowley et al., 2017; Ranney et al., 2015), so the model is known to perform well when using physically-based parameter values. The performance of the model has also been tested as the quantity of calibration data is progressively reduced, and it was shown to outperform a statistical method when using few observations for calibration (Werbylo and Niemann, 2014). However, many application regions have no point observations available for calibration, so parameters may need to be inferred from global soil, vegetation, and climatic datasets. Such datasets typically have coarse resolutions and their information inevitably includes some degree of inaccuracy. Furthermore, they do not necessarily provide the precise information that is needed to estimate the EMT+VS model parameters.

Little research has focused on the role of calibration in the application of soil moisture downscaling methods. Satellite methods that use optical/thermal data have typically been applied

without calibration to local soil moisture observations (Carlson, 2007; Chauhan et al., 2003; Kim and Hogue, 2012; Merlin et al., 2013; Piles et al., 2016), but recent research suggests that optical/thermal soil moisture estimates may require calibration to achieve adequate performance in some cases (Alburn et al., 2015). Land-surface models have also been used for downscaling without calibration (Ines et al., 2013; Sahoo et al., 2013; Verhoest et al., 2015), but some of these models exhibit biases in their soil moisture that may require calibration to overcome (De Lannoy et al., 2007; Kumar et al., 2006). Few studies have explicitly compared calibrated and uncalibrated performance for a given downscaling method. Notably, Ines et al. (2013) compared their deterministic downscaling method when it was optimized with *in situ* data and when it was optimized with idealized experiments. Peng et al. (2017) summarizes the current state of knowledge as follows: "…each method has its applicability under certain purposes, and over different surface and climate conditions, none of the methods can be applied everywhere over the world without any calibration or improvements."

The objectives of this research are (1) to develop methods for estimating the EMT+VS model parameters from global soil, vegetation, and climatic datasets and (2) to characterize the model performance when its parameters are determined from currently available datasets instead of site-specific calibration. The outline of the paper is as follows. Section 2 briefly describes the EMT+VS model and highlights its parameters. Section 3 summarizes the four small catchments and two large regions where the study is performed and presents the model application methods. Section 4 describes the global datasets that are used and how reference parameter values are obtained from those datasets. Section 5 compares the reference parameter values to the calibrated parameter values and identifies the datasets that can be used to estimate parameters. Section 6

develops recommended parameter values, and Section 7 evaluates the global (without site-specific calibration) model performance. Section 8 summarizes the main conclusions.

## 2. EMT+VS MODEL AND PARAMETERS

This section summarizes the EMT+VS model and identifies all its parameters. A detailed description of the EMT+VS model is provided by Coleman and Niemann (2013), Ranney et al. (2015), and Cowley et al. (2017). The EMT+VS model considers the hydrologically active layer, which is defined as the surface soil layer within which most lateral flow occurs. Specifically, it evaluates the water balance of the hydrologically active layer upslope from an edge of a fine-resolution grid cell in a digital elevation model (DEM). Four processes are included in the water balance: infiltration $F$, deep drainage $G$, lateral flow $L$, and evapotranspiration (ET) $E$ (see Appendix for List of Variables). The process descriptions are simple, particularly in regards to representing temporal variability, because the soil moisture is ultimately calculated using an equilibrium assumption.

Infiltration $F$ (mm d$^{-1}$) is described using a simple expression that can account for orographic precipitation and interception by the canopy. It can be written:

$$F = F_{\max}(1 - \lambda V) \tag{1}$$

where $F_{\max}$ (mm d$^{-1}$) is the maximum infiltration rate that depends on precipitation, $\lambda$ is the interception efficiency of the vegetation cover (a parameter), and $V$ is the fractional vegetation cover. The parenthetical term represents the throughfall fraction. $F_{\max}$ can be spatially constant (in which case it eventually disappears from the model and does not need to be specified) or it can be calculated as a function of topographic slope, aspect, and elevation to include orographic effects (Cowley et al., 2017). Cowley et al. (2017) found that including orographic precipitation did not substantially improve calibrated EMT+VS model performance, so $F_{\max}$ is treated as a constant throughout this study.

Deep drainage $G$ (mm d$^{-1}$) is calculated from Darcy's Law with gravity drainage (no capillary gradient) and the Campbell (1974) equation for unsaturated hydraulic conductivity. It can be written:

$$G = K_{s,v}\left(\frac{\theta}{\phi}\right)^{\gamma_v} \tag{2}$$

where $K_{s,v}$ (mm d$^{-1}$) is the vertical saturated hydraulic conductivity (a parameter), $\theta$ (m$^3$ m$^{-3}$) is the volumetric water content in the modeled soil layer, $\phi$ (m$^3$ m$^{-3}$) is the soil porosity (a parameter), and $\gamma_v$ is the vertical pore disconnectedness index (a parameter).

Lateral flow $L$ (m$^2$ mm d$^{-1}$) is described using Darcy's Law, the Campbell (1974) equation for unsaturated hydraulic conductivity, a hydraulic gradient that is a power function of the topographic slope, and a soil depth that depends on topographic curvature. It can be written:

$$L = \delta_0\left(\frac{\kappa_{\min} - \kappa}{\kappa_{\min}}\right) c\iota K_{s,v}\left(\frac{\theta}{\phi}\right)^{\gamma_h} S^{\varepsilon} \tag{3}$$

where $\delta_0$ (m) is the thickness of the hydrologically active layer at locations where topographic curvature is zero (a parameter), $\kappa_{\min}$ (m$^{-1}$) is the minimum topographic curvature for which the hydrologically active layer is present (a parameter), $\kappa$ (m$^{-1}$) is the topographic curvature, $c$ (m) is the length of the DEM grid cell, $\iota$ is the anisotropy of saturated hydraulic conductivity (a parameter), $\gamma_h$ is the horizontal pore disconnectedness index (a parameter), $S$ is the topographic slope from the DEM, and $\varepsilon$ relates the horizontal hydraulic gradient to topographic slope (a parameter).

ET $E$ (mm d$^{-1}$) is modeled by inferring the spatial variations in potential ET from elevation variations, partitioning evaporation and transpiration using fractional vegetation cover, partitioning the radiative and aerodynamic components using the Priestley-Taylor (1972)

assumption, accounting for insolation variations using the potential solar radiation index (PSRI), and describing moisture limitation effects using power functions. It can be written:

$$E = \overline{E}_p \left[ 1 + \omega \left( \overline{Z} - Z \right) \right] \left[ \eta V + \left( 1 - V \right)^{\mu} \right] \left[ \frac{I_p}{1+\alpha} \left( \frac{\theta}{\phi} \right)^{\beta_r} + \frac{\alpha}{1+\alpha} \left( \frac{\theta}{\phi} \right)^{\beta_a} \right] \tag{4}$$

where $\overline{E}_p$ (mm d$^{-1}$) is the spatial average PET (a parameter), $\omega$ is the elevation dependence of PET (a parameter), $\overline{Z}$ (m) is the spatial average elevation, $Z$ (m) is the local elevation, $\eta$ is the portion of total transpiration that is contributed by the hydrologically active layer (a parameter), $\mu$ accounts for shading effects on soil evaporation (a parameter), $\alpha$ is the Priestley-Taylor coefficient minus one (a parameter), and $I_p$ is the PSRI, which depends on aspect, slope, and latitude. $\beta_r$ and $\beta_a$ characterize the moisture limitation effect in the aerodynamic and radiative terms of $E$, respectively (both are parameters).

Coleman and Niemann (2013) developed an approximate solution to the water balance where local soil moisture is calculated from a supplied spatial average (or coarse-resolution grid of) soil moisture. After assuming equilibrium, four explicit analytical solutions for soil moisture are found by assuming that each outflow term in the water balance dominates the others. The final soil moisture is then found by a weighted average of those analytical solutions where the weights are the magnitudes of the outflow terms in the water balance. The final soil moisture is:

$$\theta = \frac{w_G \theta_G + w_L \theta_L + w_R \theta_R + w_A \theta_A}{w_G + w_L + w_R + w_A} \tag{5}$$

where $\theta_G$, $\theta_L$, $\theta_R$, and $\theta_A$ are the explicit soil moisture estimates if deep drainage, lateral flow, radiative ET, and aerodynamic ET dominate, respectively, and $w_G$, $w_L$, $w_R$, and $w_A$ are associated weights. The equations for $\theta_G$, $\theta_L$, $\theta_R$, and $\theta_A$ are:

$$\theta_G = \bar{\theta}\frac{\mathrm{DDI}}{\overline{\mathrm{DDI}}} \tag{6}$$

$$\theta_L = \bar{\theta}\frac{\mathrm{LFI}}{\overline{\mathrm{LFI}}} \tag{7}$$

$$\theta_R = \bar{\theta}\frac{\mathrm{REI}}{\overline{\mathrm{REI}}} \tag{8}$$

$$\theta_A = \bar{\theta}\frac{\mathrm{AEI}}{\overline{\mathrm{AEI}}} \tag{9}$$

where $\bar{\theta}$ is the supplied spatial average soil moisture, $\mathrm{DDI}$ is the deep drainage index, $\mathrm{LFI}$ is the lateral flow index, $\mathrm{REI}$ is the radiative ET index, and $\mathrm{AEI}$ is the aerodynamic ET index. The quantities $\overline{\mathrm{DDI}}$, $\overline{\mathrm{LFI}}$, $\overline{\mathrm{REI}}$, and $\overline{\mathrm{AEI}}$ are the spatial averages of the indices.

The indices are defined:

$$\mathrm{DDI} \equiv \phi\left(\frac{1-\lambda V}{K_{s,v}}\right)^{1/\gamma_v} \tag{10}$$

$$\mathrm{LFI} \equiv \phi\left(\frac{1-\lambda V}{\delta_0 \imath K_{s,\mathrm{v}}}\right)^{1/\gamma_h}\left(\frac{A}{cS^{\varepsilon}}\right)^{1/\gamma_h}\left(\frac{\kappa_{\min}}{\kappa_{\min}-\kappa}\right)^{1/\gamma_h} \tag{11}$$

$$\mathrm{REI} \equiv \phi\left\{\frac{1+\alpha}{\bar{E}_p\left[1+\omega\left(\bar{Z}-Z\right)\right]}\right\}^{1/\beta_r}\left(\frac{1}{I_p}\right)^{1/\beta_r}\left[\frac{\left(1-\lambda V\right)}{\eta V+(1-V)^{\mu}}\right]^{1/\beta_r} \tag{12}$$

$$\mathrm{AEI} \equiv \phi\left\{\frac{1+\alpha}{\alpha\bar{E}_p\left[1+\omega\left(\bar{Z}-Z\right)\right]}\right\}^{1/\beta_a}\left[\frac{1-\lambda V}{\eta V+(1-V)^{\mu}}\right]^{1/\beta_a} \tag{13}$$

These indices are treated as temporally invariant and produce the spatial variations in the fine-scale soil moisture pattern. Those variations are produced by fine-scale variations in elevation $Z$, slope $S$, curvature $\kappa$, PSRI $I_p$, contributing area $A$, and fractional vegetation cover $V$. The associated weights can vary in time. They are:

$$w_G = \left( \frac{\bar{\theta}}{\overline{\mathrm{DDI}}} \right)^{\gamma_v} \tag{14}$$

$$w_L = \left( \frac{\bar{\theta}}{\overline{\mathrm{LFI}}} \right)^{\gamma_h} \tag{15}$$

$$w_R = \left( \frac{\bar{\theta}}{\overline{\mathrm{REI}}} \right)^{\beta_r} \tag{16}$$

$$w_A = \left( \frac{\bar{\theta}}{\overline{\mathrm{AEI}}} \right)^{\beta_a} \tag{17}$$

In the end, the key model inputs are coarse-resolution soil moisture $\bar{\theta}$, fine-resolution topographic elevation (from which the required topographic attributes are calculated), fine-resolution fractional vegetation cover $V$, and parameters. All the parameters are specified at the coarse-resolution for this study. Three parameters are related to the local climate, eight describe the local soil, and five characterize the vegetation cover. The parameters that are evaluated in this study are summarized in Table 1. The "Recommended Parameters" column in Table 1 is discussed later.

# 3. APPLICATION TO STUDY SITES

## *3.1 STUDY SITES*

The EMT+VS model is tested using four small catchments and two large regions (Figure 1). The catchments (Tarrawarra, Satellite Station, Cache la Poudre, and Nerrigundah) have diverse soil moisture patterns (Ranney et al., 2015) and gridded soil moisture observations available for model calibration and evaluation. The two large regions (Reynolds Creek and Tibet) also have different soil moisture patterns but fewer soil moisture observations than the catchments. These study sites were selected because the observation locations capture some of the regional variation in topographic attributes and vegetation density, so they are expected to capture more spatial variability in soil moisture than some other available datasets. All of these sites except for Tibet have been used previously to evaluate the calibrated EMT+VS model.

The Tarrawarra dataset was originally described by Western and Grayson (1998). This 10.5 ha catchment is located in Victoria, Australia. It has an average annual rainfall of about 820 mm and an average potential ET of about 830 mm. The DEM was originally produced by a total station survey and has a 5 m resolution. The vegetation is grazed grass. The soil moisture dataset was collected using time domain reflectometry (TDR) in the top 30 cm of the soil. Observations were collected on a 10 m by 20 m grid on 13 dates spanning 14 months in 1995 and 1996. The soil moisture patterns in this catchment are temporally unstable with both valley dependent and hillslope dependent patterns occurring (Western et al., 1999; Wilson et al., 2005).

The Satellite Station dataset was originally presented by Wilson et al. (2003). The 60 ha catchment is located on the North Island of New Zealand. It has an average annual rainfall of approximately 1600 mm and annual pan evaporation of approximately 1300 mm. The DEM was

originally produced by a total station survey and has a 10 m resolution. The vegetation is primarily grazed grass. The soil moisture dataset was collected using TDR and characterizes the top 30 cm of the soil. The observations were collected on a 40 m grid on 6 dates spanning 20 months in 1998 and 1999. The soil moisture patterns in this watershed are valley dependent (Coleman and Niemann, 2013).

The Cache la Poudre dataset was originally described by Coleman and Niemann (2012). The 8 ha catchment is located in Colorado, USA. It has an average annual precipitation of about 400 mm and annual PET of about 930 mm. The DEM was originally produced by a land survey and has a 15 m resolution. Vegetation is aspect dependent with shrubs on south-facing slopes and coniferous trees on north-facing slopes. The soil moisture dataset was collected using TDR and describes the top 5 cm of the soil. Observations were collected on a 15 m grid on 9 dates spanning 3 months in 2008. The soil moisture in this watershed is hillslope dependent (Coleman and Niemann, 2012).

The Nerrigundah dataset was originally described by Walker et al. (2001). The 6 ha catchment is located near Dungog, New South Wales, Australia. It has an average annual precipitation of about 1000 mm and a class A pan evaporation of about 1600 mm. The DEM was originally produced by a total station survey and has a 20 m resolution. The vegetation is primarily grazed grass. The soil moisture dataset was collected using TDR and is available for the top 15 cm on a 20 m grid. Observations were collected on 12 dates that span 2 months in 1997. Like Satellite Station, the soil moisture patterns in this watershed are valley dependent (Ranney et al., 2015).

The Reynolds Creek dataset was summarized by Seyfried et al. (2001) and is a SMAP validation site (Colliander et al., 2017). This 239 $km^2$ watershed is located in Idaho, USA. It has

an average annual precipitation that varies from 230 mm at lower elevations to 1100 mm at higher elevations (Hanson, 2001), and an average pan evaporation of about 1044 mm (Hanson, 1989). The DEM was obtained from the United States Geological Survey National Map Viewer and has a 30 m resolution. The vegetation is mostly sagebrush with some aspen and firs at higher elevations. The soil moisture dataset is from 30 permanently installed Hydra Probes and characterizes the top 5 cm of the soil (Seyfried et al., 2005; Seyfried and Murdock, 2004). The observations used here are from 30 dates in May and June from 2012 to 2014. The soil moisture patterns in this watershed are primarily elevation dependent (Cowley et al., 2017).

The Tibet dataset was originally described by Yang et al. (2013) and is a SMAP validation site (Jackson et al., 2016). This 1960 $km^2$ region is located in Nagqu, China. It has an average annual precipitation of about 500 mm and an average annual PET of about 850 mm (Zhang et al., 2009). The DEM was obtained from Advanced Spaceborne Thermal Emission and Reflection Radiometer (ASTER) Global Digital Elevation Model (GDEM) V2 and has a 30 m resolution. The vegetation is predominantly short alpine grasses. The soil moisture is characterized using 29 permanently installed capacitance probes and characterizes the top 5 cm of the soil. The observations used here are from 31 dates during June through September from 2011 to 2012.

### *3.2 MODEL APPLICATION*

In order to apply the EMT+VS model to the study sites, the following data must be provided: coarse-resolution soil moisture $\overline{\theta}$, fine-resolution topographic and fractional vegetation cover $V$ data, and the model parameters. For this study, $\overline{\theta}$ was calculated as the spatial average of the *in situ* soil moisture observations. This approach ensures that $\overline{\theta}$ is as

accurate as possible and that the comparison between the locally calibrated and global models does not depend on a particular technology used to determine $\bar{\theta}$. The topographic attributes were calculated from the local DEMs described in the previous section, ensuring proper alignment between the gridded soil moisture observations and the downscaled patterns. Fractional vegetation cover $V$ was estimated using the soil adjusted vegetation index (SAVI) (Huete, 1988) following Cowley et al. (2017). The SAVI was calculated from Landsat images on dates without cloud cover during the period of soil moisture data collection. Because the four catchments are so small, only a single spatial average $V$ is used. For Tarrawarra, the Landsat 5 image is from 8 October 1995, and $V$ = 0.60. For Satellite Station, the Landsat 5 image is from 19 November 1992, and $V$ = 0.54. For Cache la Poudre, the Landsat 5 image is from 26 June 2006, and $V$ = 0.22. For Nerrigundah, the Landsat 5 image is from 21 August 1997, and $V$ = 0.34. For the two large regions, fine-resolution patterns are used for $V$. For Reynolds Creek, $V$ was found by averaging the results from Landsat 8 images on 05 June 2013, 08 June 2014, and 11 June 2015. For Tibet, $V$ was found by averaging the results from Landsat 7 images on 17 June 2011, 29 August 2011, and 14 September 2011.

For the calibrated model cases, the parameter values were adjusted to maximize model performance. Model performance was quantified by calculating the Nash Sutcliffe Coefficient of Efficiency (NSCE) (Nash and Sutcliffe, 1970) for each date (referred to as the spatial NSCE) and then averaging. For a given date, a spatial NSCE of 1 indicates that the downscaling model perfectly reproduces the soil moisture observations. For comparison, if downscaling was not implemented and $\bar{\theta}$ was used as a soil moisture model, then the NSCE would be equal to 0.Thus, an NSCE above 0 indicates that the downscaling model has less error than using $\bar{\theta}$ as the soil moisture pattern. The feasible range for each parameter was based on locally available

information about the physical characteristics (Carsel and Parrish, 1988; Cosby et al., 1984; Dingman, 2015). Three parameters were not calibrated, following previous research (Coleman and Niemann, 2013; Ranney et al., 2015). The Priestley-Taylor coefficient minus one $\alpha$ was set to 0.26, the depth of the hydrologically active layer where topographic curvature is zero $\delta_0$ was set based on local knowledge of the soil layer, and $\overline{E}_p$ was calculated based on local meteorological data. The calibrated model results that are presented later in this paper differ from previous studies. Here, the model inputs were selected to be more consistent between study sites and to be more representative of what might be available in data sparse regions. For example, SAVI is used to characterize vegetation at all sites, whereas previous calibrations sometimes neglected vegetation and sometimes used local vegetation datasets. Also, previous calibrations did not always include elevation dependence in the calculation of potential ET.

# 4. REFERENCE PARAMETER VALUES

For the global application of the model (without site-specific calibration), initial estimates of the parameters (reference values) were obtained from global datasets. To be considered for this study, a dataset was required to have global coverage, to be free of charge, and to be publically available. Among the identified alternatives, the final dataset was chosen based on its accuracy and spatial resolution.

## *4.1 CLIMATE PARAMETERS*

Spatial average potential ET $\overline{E}_p$ was obtained from the Consultative Group for International Agriculture Research Consortium for Spatial Information (CGIAR-CSI) (Trabucco et al., 2008). Compared to the MODerate resolution Imaging Spectroradiometer (MODIS) global ET from the University of Montana (Mu et al., 2011), CGIAR-CSI produced better estimates when compared to the $\overline{E}_p$ values calculated from meteorological data for the study sites. CGIAR-CSI calculated potential ET using the Hargreaves equation, WorldClim meteorological data, and Shuttle Radar Topography Mission (SRTM) DEM data. The dataset provides annual and monthly averages from 1950 to 2000 at a 30 arc-second (~1 km) resolution. For $\overline{E}_p$, the average value over the entire time period was calculated for each study site with the annual average dataset.

The elevation dependence of potential ET $\omega$ is not directly available from any identified dataset, but we investigate if it can be estimated from other available data. An analysis was performed at Reynolds Creek because it has 17 meteorological stations at different elevations with measurements of air temperature, vapor pressure, relative humidity, incoming solar

radiation, and wind speed (Hanson et al., 2001). Using this data, daily ASCE short grass standardized reference ET (Walter et al., 2000) was calculated for 2012 and 2013 and used as an estimate of potential ET. For each day, the potential ET was plotted against elevation and used to estimate $\omega$ on that day. The dependence of the daily $\omega$ values on various daily meteorological conditions was then examined. Empirically, wind speed exhibits the strongest relationship with potential ET among the variables considered (and this dependence can be seen in the equations used to obtain reference ET as well). Figure 2 shows the $\omega$ values plotted as a function of the wind speed and the fitted zero-intercept linear relationship. The relationship is:

$$\omega = 0.00018 * W \tag{18}$$

where $\omega$ has units of $m^{-1}$ and $W$ is the average wind speed ($m\ s^{-1}$). This relationship has a coefficient of determination ($r^2$) of 0.36 and can potentially be used to estimate $\omega$ at any study site based on the local wind speed. A logarithmic nonlinear relationship was also considered but it produced similar $\omega$ values for the six study sites.

Global wind speed data were obtained from the National Centers for Environmental Prediction (NCEP) Climate Forecast System Reanalysis (CFSR) (Saha et al., 2010). This dataset is based on observations and a coupled atmosphere-ocean-land surface-sea ice modeling system. It has been shown to be a viable alternative when direct observations are not available for the variables of interest (Dile and Srinivasan, 2014; Fuka et al., 2014). The dataset provides daily wind speed data at a 38 km resolution from 1979 to 2014. To estimate $\omega$, we used the average reported daily wind speed for the entire time period of the dataset.

No global datasets were found to allow regional estimation of $\alpha$. However, multiple authors have supported the assumption that $\alpha$ is approximately constant at 0.26 (Dingman, 2015; Ershadi et al., 2014; Mu et al., 2011). Furthermore, 0.26 has been used in calibrated

applications of the EMT+VS model (Coleman and Niemann, 2013; Cowley et al., 2017; Ranney et al., 2015), so 0.26 is also assumed for the global cases.

*4.2 SOIL PARAMETERS*

Soil characteristics were obtained from the International Soil Reference and Information Centre World Inventory of Soil property Estimates (ISRIC-WISE) (Batjes, 2015), who released an update to the Harmonized World Soil Database (FAO et al., 2012). Other soil datasets are available, but they either have issues with quality control like the Global Soil Dataset for Earth System Modeling (Shangguan et al., 2014) or remain unfinished like the Global Soil Map (Sanchez et al., 2009). The ISRIC-WISE database provides soil properties at a 30 arc-second (~1 km) resolution (Batjes, 2015). Data provided in the database includes bulk density, organic carbon content, and percent sand, silt, clay, among many others.

The ISRIC-WISE percent sand, silt, clay, and organic carbon content were used in the Saxton and Rawls (2006) pedotransfer functions to estimate porosity $\phi$, vertical saturated hydraulic conductivity $K_{s,v}$, and vertical pore disconnectedness $\gamma_v$. Note that we assume that the pedotransfer functions describe the vertical properties. The Saxton and Rawls (2006) functions were selected because they are based on more soil samples than, for example, the Cosby et al. (1984) pedotransfer functions. The Cosby et al. (1984) functions also produced similar values for the hydraulic properties. The porosity $\phi$ is calculated:

$$\phi = \theta_{33} + \theta_{(S-33)} - 0.097 * S + 0.043 \tag{19}$$

where $S$ is the percentage of sand, $\theta_{33}$ is the field capacity, and $\theta_{(S-33)}$ is the saturated soil moisture minus field capacity. The $\theta_{33}$ and $\theta_{(S-33)}$ values can be determined with other equations from Saxton and Rawls (2006). $K_{s,v}$ is calculated:

$$K_{s,v} = 1930(\phi - \theta_{33})^{(3-1/B)} \tag{20}$$

$$B = (\ln 1500 - \ln 33)/(\ln \theta_{33} - \ln \theta_{1500}) \tag{21}$$

where $B$ is the pore size distribution index and $\theta_{1500}$ is the wilting point. Both $B$ and $\theta_{1500}$ can be calculated from Saxton and Rawls (2006). Finally, $\gamma_v$ is found from:

$$\gamma_v = 2B + 3 \tag{22}$$

Anisotropy $\iota$ is not available from the ISRIC-WISE dataset, but we investigate if it can be estimated by matching the extents of saturated valley bottoms to observed stream extents. This approach is based on the simplified conceptual model that a stream forms where the soil is continuously saturated. In reality, soil may not even be present where streams occur (e.g., bedrock rivers), and streams are often sustained by groundwater discharge rather than saturated soil. Observed stream extents were obtained from the USGS-generated Hydrological data and maps based on SHuttle Elevation Derivatives at multiple Scales (HydroSHEDS) (Lehner et al., 2008). This vector dataset has a resolution of 15 arc-seconds (~500 m). It is based on SRTM DEM data, Water Body Data, Digital Chart of the World rivers and lakes data, the ArcWorld global vectorized river network, and the Global Lakes and Wetlands Database. Previous results show an accuracy that significantly exceeds other global watershed and river maps (Lehner et al., 2008). To estimate $\iota$, the other EMT+VS parameters were set to their reference values and $\bar{\theta}$ was set to the average among the dates in each study site's dataset. As the parameter $\iota$ increases, the valley bottoms become saturated further up towards their headwaters. $\iota$ was increased until

the saturated valley bottoms matched the stream extents. This value was selected as the reference value. The small catchments do not include streams, so the area was extended to a 0.25° x 0.25° square centered on the original catchment for estimating $t$.

No global datasets were found to estimate $\delta_0$, $\kappa_{\min}$, $\gamma_h$ and $\varepsilon$. Several authors assume a typical rooting depth or soil thickness of 30 cm (Jackson et al., 2000; Porporato et al., 2004; Schenk and Jackson, 2002), which would imply that $\delta_0$ is near that value. Also, $\delta_0$ only appears in the model with $iK_{s,v}$, which can vary over a much larger range than $\delta_0$. So, $\delta_0$ is assumed to be 30 cm in the global model for simplicity. Any dependence of soil thickness on topographic curvature is usually neglected in such models, which would suggest that $\kappa_{\min}$ has a very large negative value. Past calibrations of the EMT+VS model have also found large negative values, so $\kappa_{\min}$ is assumed to be -999,999 $m^{-1}$ in the global model. The values of $\gamma_h$ and $\varepsilon$ potentially have larger effects on the model results, so their values will be investigated later in the paper.

*4.3 VEGETATION PARAMETERS*

The vegetation parameters are expected to depend mainly on the vegetation type, so we investigate if they can be estimated from land cover classifications. The selected land cover dataset is from MODIS (Friedl et al., 2010). This dataset provides land cover classification (among other information) at a 500 m resolution. The land cover is classified into 17 categories as defined by the International Geosphere Biosphere Programme (IGBP) (Loveland and Belward, 1997). The classification is reported to have about a 75% accuracy (Friedl et al., 2010), which is competitive with other land cover classification datasets (Grekousis et al., 2015) such as GlobCover, GLC-SHARE, and GLCC (Bontemps et al., 2011; Latham et al., 2014; Loveland et

al., 2000). The MODIS dataset was selected because it exhibits the best accuracy for the study sites.

We investigate if the interception efficiency $\lambda$ can be estimated from the land cover classifications using an approach from Galdos et al. (2012). They studied interception in a manner that is consistent with the EMT+VS model for 11 land cover classifications in Northern Spain. Their categories do not perfectly align with the IGBP classifications, but they are similar enough to be matched. For each land cover, Galdos et al. (2012) provided an empirical power function that calculates the interception fraction from the gross daily rainfall. This interception fraction implicitly depends on the local fractional vegetation cover, which is considered separately in the EMT+VS model. Thus, the interception fraction is divided by the provided mean fractional vegetation cover to obtain $\lambda$ for each classification. The resulting $\lambda$ still depends on the gross rainfall, so global daily rainfall data were obtained from land-based weather stations of National Oceanic and Atmospheric Administration (NOAA) National Centers for Environmental Information (NCEI) Global Historical Climate Network (GHCN) (Peterson and Vose, 1997). For each study site, daily $\lambda$ values were calculated for the length of the available rainfall data. The average $\lambda$ was then determined by weighting the daily $\lambda$ values by the daily precipitation.

We investigate if the portion of transpiration from the modeled soil layer $\eta$ can be estimated based on Jackson et al. (1996). They analyzed root distribution data from around the world to generate equations for cumulative root fraction as a function of depth for 11 terrestrial biomes. These biomes are not perfectly consistent with the IGBP land cover classifications, but the classifications for the study sites are among the 11 biomes considered. To estimate $\eta$, it is assumed that the portion of transpiration from the layer is the same as the portion of the roots in

the layer, which neglects root increased root water uptake from soil layers with more available moisture (Jarvis, 1989).

In the EMT+VS model, different moisture limitation functions are allowed for the aerodynamic and radiative components of ET, and those functions are controlled by $\beta_a$ and $\beta_r$, respectively. Other similar models instead allow different functions for evaporation and transpiration (Ek et al., 2003; Laio et al., 2001; Rosero et al., 2010; van der Velde et al., 2009). The EMT+VS model could be generalized to treat evaporation and transpiration separately, but this modification would introduce more parameters. Instead, we note that $\beta_a$ and $\beta_r$ are expected to depend on the relative contributions of evaporation and transpiration, and $\overline{E}_p$ may crudely indicate the importance of evaporation for a region. Figure 3 plots the calibrated $\beta_a$ and $\beta_r$ values against the reference $\overline{E}_p$ values, and a weak relationship is observed. A generalized logistic function was fitted to these data. This relationship was selected because it ensures that estimated $\beta_a$ and $\beta_r$ values always fall within their feasible range (0.2 to 5 according to Lowry (1959)). We also attempted to estimate $\beta_a$ and $\beta_r$ values from land cover classifications, but that approach was found to be less reliable.

No global datasets were found to estimate the shading exponent $\mu$. Appropriate values of this parameter will be evaluated later in this study.

# 5. EVALUATING REFERENCE PARAMETERS

The accuracy of the reference parameter values can be evaluated in part by comparing them to the calibrated parameter values. However, the calibrated values may not be the only values that allow good performance of the EMT+VS model. Good performance means that the NSCE value is near the highest value observed among all the feasible parameter sets. For example, some parameters may have little effect on the model results, so any value would allow good performance. Other parameters may be important, but a range of values may provide good performance if accommodated by certain values of other parameters (Zak and Beven, 1999).

Generalized Likelihood Uncertainty Estimation (GLUE) (Beven and Binley, 1992) was used to determine the ranges of parameter values that allow good model performance. In this procedure, parameter sets are first randomly generated within their feasible ranges. The ranges were selected to encompass all physically realistic values and not constrained by any local information. Thus, they are the same for all study sites. For each study site, 10,000 parameter sets were generated (larger numbers of parameter sets did not change the GLUE results). The likelihood of each generated parameter set was then evaluated based on its average spatial NSCE. Any parameter set whose average spatial NSCE was less than 50% of the highest average spatial NSCE was considered non-behavioral and discarded. Then, the marginal cumulative likelihood function was calculated for each parameter, and the interquartile ranges (IQRs) were identified. A narrow IQR for a parameter suggests that accurate estimation of that parameter is important because only a limited range of values allows good model performance. Note that the IQR only includes 50% of the total likelihood, so some good performing parameter sets always fall outside of this range.

Figure 4 considers the EMT+VS parameters that are related to climate. The axis limits correspond to the feasible ranges for the parameters. Each vertical error bar shows the IQR from GLUE at each study site (the horizontal coordinate is the reference parameter value at that site). The individual symbols show the calibrated value at each study site. Note that the calibrated parameter value can fall outside the IQR, particularly if good performance can be achieved with a wide range of parameter values at that site. A 1:1 line is also shown in the figure. If the symbols fall near the 1:1 line, then the reference values are very similar to the calibrated values. The solid line in each plot shows the regression between the reference and calibrated values (with a zero intercept). If this line deviates from the 1:1 line, then the reference values are biased. If the points fall near the regression line (and thus the line's coefficient of determination $r^2$ is high), then the reference values are accurate estimates of the calibrated values after the bias has been corrected. Note that $r^2$ can be negative because the intercept is forced to be zero.

For the spatial average potential ET $\overline{E}_p$ (Figure 4a), the IQRs are all broad, suggesting that a wide range of $\overline{E}_p$ values can produce good model performance (i.e. average spatial NSCE values that are similar to the average spatial NSCE for the calibrated parameter set) at all sites. Thus, accurate estimation of $\overline{E}_p$ may not be critical. The regression line indicates that the reference values are typically lower than the calibrated values. However, the points are clustered near the regression line ($r^2 = 0.58$), which suggests that the calibrated $\overline{E}_p$ values can be roughly estimated from the reference values. For the elevation dependence of potential ET $\omega$ (Figure 4b), the IQRs are broad for the four catchments and narrower for the two regions. Also, the IQRs for the two large regions do not overlap. The four catchments have small elevation ranges, so $\omega$ has little effect on the model performance. The two large regions have greater topographic relief, so it is more important to estimate $\omega$ accurately. The calibrated values are far from the reference

values ($r^2$ = -1.00). This disagreement could occur because: (1) the global NCEP CFSR wind speed dataset is not accurate, (2) the wind speed relationship does not apply outside of Reynolds Creek, and/or (3) the calibrated $\omega$ values include effects beyond spatial variations in potential ET. For the time period of analysis at Reynolds Creek, the average daily wind speed is 2.5 m $s^{-1}$ from the *in situ* data and 2.9 m $s^{-1}$ from the NCEP CFSR data, which suggests that the NCEP data is not the primary source of error. However, the calibrated $\omega$ at Reynolds Creek is much higher than the value expected from the potential ET and elevation data. This difference suggests that $\omega$ includes elevation dependence in other variables such as precipitation and soil properties (Cowley et al., 2017).

The soil related parameters are evaluated in Figure 5. For porosity $\phi$ (Figure 5a), the IQRs are narrow at Tarrawarra, Satellite Station, and Tibet, but broad for the other sites. Also, the IQRs for Satellite Station and Tibet do not overlap. Both Tibet and Tarrawarra require high $\phi$ values in part because high observed soil moisture values occur at these sites. The upper limit of the calibration range was set to the maximum value of the observed soil moisture among all datasets, which is 0.70 at Tarrawarra. The reference values all fall within a very narrow range compared to the calibrated values, and no relationship exists between the reference and calibrated parameters ($r^2$ = -0.04). Overall, these results suggest site-specific $\phi$ values are required for some sites yet the reference values are not useful for estimating local $\phi$ values. For vertical saturated hydraulic conductivity $K_{s,v}$ (Figure 5b), all the IQRs are broad, which suggests a wide range of $K_{s,v}$ allows good model performance. In the EMT+VS model, $K_{s,v}$ directly affects the importance of deep drainage, but deep drainage does not introduce spatial variations in soil moisture unless the vegetation has spatial variations. $K_{s,v}$ also affects the importance of

lateral flow. However, in the lateral flow expression, $K_{s,v}$ is multiplied by $\iota$. Thus, a range of $K_{s,v}$ values can produce the same lateral flow if $\iota$ also varies to accommodate the $K_{s,v}$ values. Aside from Reynolds Creek, a moderately strong relationship is observed between reference and calibrated $K_{s,v}$ parameters ($r^2$ = 0.49 when Reynold Creek is excluded). Reynolds Creek appears to be an outlier because its value is inconsistent with the other study sites and its calibrated value is above its wide IQR. The reference $K_{s,v}$ values are typically greater than the calibrated values. Overall, the results suggest that reproduction of the calibrated $K_{s,v}$ values is not mandatory for good model performance, but the global datasets can provide reasonable estimates for most sites. For vertical pore disconnectedness index $\gamma_v$ (Figure 5c), the IQRs are relatively narrow and have different ranges for the different sites, which suggests that accurate estimation of site-specific $\gamma_v$ values is required for good model performance. The narrow range likely occurs because $\gamma_v$ has a unique role in the model equations and no other parameter can be adjusted to accommodate a given $\gamma_v$ value. The reference values are typically higher than the calibrated values, but a moderate relationship exists between the reference and calibrated parameters ($r^2$ = 0.34). Thus, $\gamma_v$ can be roughly estimated from the global dataset. For anisotropy $\iota$ (Figure 5d), the IQRs are consistently broad, suggesting that a wide range of values allows good model performance. However, no relationship exists between reference and calibrated parameter values ($r^2$ = -0.54), which suggests that estimating $\iota$ by matching stream extents is unreliable.

The vegetation related parameters are evaluated in Figure 6. For interception efficiency $\lambda$ (Figure 6a), the IQRs are broad except for Tibet, but Tibet's calibrated value still falls outside its IQR. These features suggest that a wide range of values allow good model performance. No

relationship exists between reference and calibrated parameters ($r^2$ = -1.36). For the portion of transpiration derived from the modeled soil layer $\eta$ (Figure 6b), the IQRs are broad except for Tibet, but its calibrated value again falls outside its IQR. These features suggest that a wide range of values again allow good model performance. Note that the reference value depends on land cover classification, so study sites with the same classification also have the same reference value. No relationship exists between the reference and calibrated parameter values ($r^2$ = 0.11). For the aerodynamic ET exponent $\beta_a$ (Figure 6c), the IQR for Tibet is very narrow and the IQR for Reynolds Creek is also somewhat narrow, so accurate estimation of $\beta_a$ is important for these two sites. However, the reference values are typically similar to the calibrated values ($r^2$ = 0.53) with little bias. Thus, $\beta_a$ can be roughly estimated from its relationship with $\overline{E}_p$. For the radiative ET exponent $\beta_r$ (Figure 6d), the IQRs are fairly narrow for all sites, which suggests that accurate estimation of $\beta_r$ values is important. A strong relationship exists between the reference and calibrated values ($r^2$ = 0.92) with little bias, which suggests that $\beta_r$ can be estimated from $\overline{E}_p$ as described earlier in this study.

Figure 7 examines the three parameters without reference values to determine whether they can be assumed to be constant across all sites. For the horizontal pore disconnectedness index $\gamma_h$, the IQRs are broad except for Satellite Station, where the IQR is quite narrow. Thus, assuming a constant value will produce errors at this catchment unless its preferred range of values is selected. For $\varepsilon$ and $\mu$, the IQRs are all broad. For $\mu$, Tibet exhibits a smaller IQR, but its range overlaps the ranges for the other study sites. Thus, constant values can likely be assumed for both $\varepsilon$ and $\mu$.

# 6. RECOMMENDED PARAMETERS

The previous section suggested that $\bar{E}_p$, $K_{s,v}$, $\gamma_v$, $\beta_a$, and $\beta_r$ could be roughly estimated from the global datasets, while the other parameters must be assumed to be constant. The reference values were also found to exhibit biases compared to the calibrated values in some cases. This section identifies recommended parameter values for use in the global EMT+VS model using an optimization method. If relationships were seen between the reference and calibrated values in the previous section, then the reference values are used to determine recommended values. Otherwise, a global constant is used as the recommended value.

For $\bar{E}_p$, $K_{s,v}$, $\gamma_v$, the recommended parameter value $P_{recommended}$ is found from:

$$P_{recommended} = \psi_P P_{reference}$$

where $\psi_P$ is a site-independent adjustment factor and $P_{reference}$ is the reference parameter value from the global dataset. The adjustment factors are control variables in the optimization. They aim to overcome biases in the reference values and select parameter values that are compatible with the other parameter values of the model. For $\beta_a$ and $\beta_r$, the center and rate parameters of the generalized logistic functions are also control variables, but the feasible limits are fixed at 0.2 and 5.0. For the remaining parameters, the constant values are included as control variables, but the constants are constrained within each parameter's feasible limits.

The objective function is:

$$f_{obj} = \left(\frac{1}{N}\right)\left(\frac{NSCE_{global,1}}{NSCE_{cal,1}} + \frac{NSCE_{global,2}}{NSCE_{cal,2}} + \ldots + \frac{NSCE_{global,i}}{NSCE_{cal,i}}\right) \quad (23)$$

where $f_{obj}$ is the overall fraction of the average spatial NSCE that is retained by the global model, $NSCE_{global,i}$ is the average spatial NSCE for the global model at study site $i$, $NSCE_{cal,i}$ is the average spatial NSCE for the calibrated model at study site $i$, and $N$ is the total number of study sites. The initial values for the control variables were randomly generated within their feasible limits and the sequential quadratic programming optimization was repeated 50 times.

The final recommended parameters are summarized in Table 1. Considering the climate parameters first, the recommended $\overline{E}_p$ values are much lower than the reference values (the adjustment factor is 0.48). Although Figure 4a showed that the reference values are higher than the calibrated values, the bias was not so large. The low $\overline{E}_p$ values reduce the overall variation in the global EMT+VS soil moisture patterns, which tends to reduce errors when they occur. The recommended $\omega$ value is similar to the calibrated value at Tibet but much lower than the value for Reynolds Creek.

For the soil parameters, the recommended $\phi$ value is reasonable but low compared to the IQRs for Tarrawarra and Tibet (Figure 5a). The lower $\phi$ constrains the range of EMT+VS soil moisture values and reduces the possibility of large errors. The adjustment factors for vertical saturated hydraulic conductivity $K_{s,v}$ and vertical pore disconnectedness index $\gamma_v$ are slightly greater than 1, which is expected from Figures 5c and 5d. The recommended $\gamma_h$ value is within the narrow IQR for Satellite Station, which is the only site with a narrow IQR for this variable (Figure 7a). The recommended $\iota$ of 375 falls within the broad IQRs seen in Figure 5d, but it is higher than expected for typical soils (Maidment, 1993). The recommended $\varepsilon$ value is towards the lower end of the IQRs in Figure 5c. This low value reduces the nonlinearity in the slope dependence (Equation 3), which likely reduces the magnitude of errors when they occur.

For the vegetation parameters, the recommended $\lambda$ value is realistic and falls within all the IQRs. The recommended $\eta$ value is high because it suggests that almost all transpired water is drawn from the top 30 cm of the soil. The recommended $\mu$ value falls near the upper end of the IQRs in Figure 7c and near the calibrated values for four of the six study sites. The parameters for the generalized logistic functions produce $\beta_a$ and $\beta_r$ values that are similar to the calibrated values.

# 7. GLOBAL MODEL PERFORMANCE

This section evaluates the performance of the global model. Figure 8 compares the soil moisture patterns from the observations, locally calibrated EMT+VS model, and global EMT+VS model for an example date at each of the four small catchments. Figure 9 compares the locally calibrated and global EMT+VS soil moisture patterns for example dates at the two large regions (the observed patterns cannot be shown due to the sparseness of the observations). For all cases, the global model's patterns use the recommended parameter values. Overall, the global model's soil moisture patterns usually preserve the main features in the calibrated patterns and observations. For example, the global model's pattern at Satellite Station exhibits wetter locations in the valleys (valley dependence) and the global model's pattern at Cache la Poudre exhibits wetter locations on the north-facing hillslope (hillslope dependence) like their respective observations. For Tibet, both the calibrated and global model's patterns exhibit a strong dependence on the fractional vegetation cover. The global model is less successful at Tarrawarra, where the global model's soil moisture has much less spatial variation than the observations and calibrated model. It is also less successful at Reynolds Creek where the calibrated soil moisture exhibits a strong elevation dependence while the global model's soil moisture exhibits a strong hillslope dependence. The poor performance at Reynolds Creek occurs because the $\omega$ values that allow good performance at Reynolds Creek and Tibet are inconsistent. The recommended constant value can only allow good performance at one of the two sites. Thus, it is important to find a way to estimate site-specific $\omega$ values from global datasets to improve performance.

The spatial structure of the EMT+VS soil moisture patterns is largely controlled by the relative weights in the model (Equations 14 to 17) (Coleman and Niemann, 2013). For example,

large $w_L$ values emphasize lateral flow and tend to produce valley dependence, while large $w_R$ values emphasize radiative ET and tend to produce hillslope dependence. Figure 10 plots the relative weights at each study site as a function of the spatial average soil moisture for both the global and calibrated models. The weights differ quantitatively due to differences in the parameter values, but the correct processes tend to be emphasized as the spatial average soil moisture changes for most sites. This similarity explains why the global model's soil moisture patterns are visually similar to the calibrated patterns for most cases. Reynolds Creek has the largest difference between the weights for the locally calibrated and global models, which explains why the calibrated and global soil moisture are visually dissimilar.

Figure 11 compares the spatial NSCE values for the calibrated and global models on each date for the study sites. For the calibrated model, the spatial NSCE value is positive for nearly every date at every study site. A positive spatial NSCE value means that the model reproduces the observations better than if $\bar{\theta}$ was used as the fine-resolution pattern. The global model shows a substantial reduction in spatial NSCE values and exhibits more days with negative spatial NSCE values. For Reynolds Creek, the spatial NSCE is near zero on all dates. The low performance is expected from the difference between the calibrated and global soil moisture patterns shown earlier. For Tibet, good performance occurs on dry dates but not for wet dates. The performance at Tarrawarra also decreases for wet dates. This result may occur because the recommended $\phi$ is lower than some soil moisture observations for wet dates at these sites. Overall, however, most dates continue to exhibit positive spatial NSCE values, which suggests that the global EMT+VS patterns are more accurate than the coarse-resolution input.

Figure 12 compares the performance of the locally calibrated and global models when all dates are combined together. Figure 12a shows the average spatial NSCE, which characterizes

the EMT+VS model's ability to reproduce observed spatial variations in soil moisture. Overall, the global model retains about 52% of the calibrated model's average spatial NSCE for the four small catchments. While the average spatial NSCEs remain positive for the two large regions, the reduction in performance is larger. As seen earlier, the low performance at Reynolds Creek occurs because the global model emphasizes hillslope dependence more than elevation dependence. The low performance at Tibet primarily occurs because the global model does not reproduce the unusually high soil moisture values that occur for wet conditions. Overall, 38% of the calibrated model's average spatial NSCE is retained by the global model.

Figure 12b shows the space-time NSCE, which combines all soil moisture observations from a given study site into a single NSCE calculation. This calculation method is more consistent with typical applications of NSCE in hydrologic modeling and characterizes the downscaling method's ability to reproduce both the spatial and temporal variations in the observed soil moisture. The model captures much of the temporal variability in the soil moisture patterns because the spatial average soil moisture is provided to the model as its key input. Thus, the space-time NSCE values are higher than the spatial NSCE values. Only Reynolds Creek performs poorly when overall variability of soil moisture is considered. Overall, 82% of the calibrated model's space-time NSCE is retained by the global model.

It is conceivable that the global model maintains good performance by underestimating the spatial variations in soil moisture. For example, the spatial NSCE would be zero if the downscaling method simply returns the coarse-resolution (average) soil moisture as the fine-resolution pattern. To investigate this possibility, Figure 12c compares the average spatial standard deviation of soil moisture $\sigma$ for the calibrated and global models. In all cases, $\sigma$ is smaller for the global model than the calibrated model. Overall, the global $\sigma$ is on average 58%

of the calibrated $\sigma$. Thus, the global model typically underestimates the spatial variation but still reproduces a substantial portion of the calibrated model's spatial variation. The global model exhibits the lowest NSCE values at Reynolds Creek, but it retains a larger portion of the calibrated model's $\sigma$ for this site than all other study sites except for Tarrawarra.

The root mean square error (RMSE) was also calculated for the calibrated and global models at each study site to measure the accuracy of the soil moisture estimates, as summarized in Table 2. The RMSE values at Tarrawarra and Cache la Poudre are comparable to the commonly-reported TDR measurement errors of +/- 0.03 $m^3$ $m^{-3}$ (Huisman et al., 2001). The RMSE values at Satellite Station and Nerrigundah are comparable to the SMAP mission requirement of 0.04 $m^3$ $m^{-3}$ (Das et al., 2011), while Reynolds Creek and Tibet have higher errors. Both the calibrated and global models have lower errors for the smaller catchments than the larger regions, likely because the larger regions have more heterogeneity that is not captured using spatially uniform parameters. Similarly, the difference in RMSE between the calibrated and global models is less for the small catchments than the large regions.

The preceding analyses included all study sites to evaluate the global model. Because all study sites were included in the development of the recommended parameters, the model evaluation is not completely independent from its development. It is difficult to perform extensive split sample testing because the number of study sites is small and most study sites have distinctive features. However, to provide an independent evaluation, Nerrigundah was excluded from the development of the recommended parameters and used as a validation site. Nerrigundah was selected as the validation site because it has few distinctive features in its soil moisture patterns. Thus, the remaining sites still capture the range of soil moisture patterns and allow estimation of recommended parameters. When Nerrigundah is used for validation, the

global model retains 37% of the average spatial NSCE, 83% of the space-time NSCE, 28% of the average standard deviation. The average RMSE is 0.044 $m^3$ $m^{-3}$. Thus, the performance is reduced compared to the earlier evaluation (Figure 12), but the global model still provides more accurate soil moisture estimates than the coarse-resolution input while introducing spatial variability.

# 8. CONCLUSIONS

This study developed procedures to estimate EMT+VS model parameters from global datasets and evaluated the model performance when these values are used instead of calibrated values. It also used GLUE to determine the ranges of parameter values that allow good model performance at each study site. Based on the results, the following conclusions can be made:

1. GLUE produces wide IQRs for most parameters in the EMT+VS model. Specifically, $\bar{E}_p$, $K_{s,v}$, $\iota$, and $\varepsilon$ have wide IQRs at all study sites, and $\lambda$, $\eta$, $\gamma_h$, and $\mu$ have wide IQRs at all but one study site. A wide IQR means the EMT+VS model can achieve good results (as measured by the average spatial NSCE) using a wide range of values for that parameter. In some cases, this property might occur because the parameter does not affect the model results, while in other cases, it might occur because the value of this parameter can be accommodated by adjusting the values of other parameters. A wide IQR is helpful for using the EMT+VS model in a global manner. For example, if a site-specific value cannot be estimated for a parameter, it is possible that a constant value can be used. Similarly, if the global value does not exactly match the calibrated value, the model is still likely to be able to maintain good performance. In contrast, GLUE produces narrow IQRs for $\omega$, $\phi$, $\gamma_v$, $\beta_a$, and $\beta_r$ at multiple study sites. Errors in the values of these parameters are more likely to cause EMT+VS model performance to deteriorate, so it is important for the global values of these parameters to be accurate.
2. The identified global datasets are only useful for estimating $\bar{E}_p$, $K_{s,v}$, $\gamma_v$, $\beta_a$, and $\beta_r$. In particular, the CGIAR-CSI potential ET values provide reasonable approximations of the potential ET values that were calculated from local meteorological data at the study sites.

In addition, the CGIAR-CSI potential ET values can be used in generalized logistic functions to estimate $\beta_a$ and $\beta_r$. The ISRIC-WISE soil database can be used with pedotransfer functions to approximate $K_{s,v}$ and $\gamma_v$. However, all parameter estimates that were derived from the MODIS land cover data are highly inaccurate. Neither $\omega$ or $\phi$ could be reliable estimated from the global datasets, but their values are important for achieving good model performance. Thus, future research should focus on methods for determining reliable local values for these variables.

3. When the parameter values are estimated from the global datasets using the recommended procedures, the EMT+VS model still provides value as a downscaling method. In particular, the generated fine-resolution soil moisture patterns are more accurate than the coarse-resolution input in most cases. Overall, 38% of the calibrated model's average spatial NSCE is retained by the global model, and 82% of the calibrated model's space-time NSCE is retained by the global model. The global model also continues to introduce substantial spatial variations in the soil moisture patterns, but it is lower than the calibrated model. Overall, 58% of the calibrated model's soil moisture standard deviation is retained by the global model.

Overall, the results suggest that the EMT+VS model can be used without local calibration, which potentially allows it to be applied to many more locations around the world. The recommended parameters presented here are restricted to cases like those considered, but the method used to develop their values can be used to improve the recommended values as more datasets become available. Thus, more work is needed to develop a method that truly can be used everywhere without calibration or improvement (the aspiration expressed by Peng et al. (2017)). Future work should expand the number of study sites to include a greater diversity of climatic,

soil, and vegetation conditions. For example, agricultural, thickly forested, and tropical sites have not been considered. In addition, if the larger set included multiple study sites with each type of soil moisture pattern, it would allow more split sample testing (i.e. the use of multiple independent validation sites). Future research should also consider new datasets as they become available. No global vegetation datasets were used to determine the recommended parameter values, but vegetation properties are expected to be important to the values of several parameters.

TABLES AND FIGURES

Table 1. Summary of EMT+VS model parameters and recommended values.

| Category | Parameter | Symbol | Recommended Value | Units |
|---|---|---|---|---|
| Climate | Coarse potential ET | $\overline{E}_p$ | 0.48*Reference $\overline{E}_p$ * | mm $d^{-1}$ |
| | PET elevation dependence | $\omega$ | 0.00017 | $m^{-1}$ |
| Soil | Porosity | $\phi$ | 0.48 | $m^3 m^{-3}$ |
| | Vertical saturated hydraulic conductivity | $K_{s,v}$ | 1.17* Reference $K_{s,v}$ † | mm $d^{-1}$ |
| | Vertical pore disconnectedness | $\gamma_v$ | 1.07* Reference $\gamma_v$ † | |
| | Horizontal pore disconnectedness | $\gamma_h$ | 12.05 | |
| | Anisotropy of saturated hydraulic conductivity | $\iota$ | 375 | |
| | Relation of hydraulic to topographic gradient | $\varepsilon$ | 1.33 | |
| Vegetation | Interception efficiency | $\lambda$ | 0.36 | |
| | Portion of transpiration from soil layer | $\eta$ | 0.98 | |
| | Shading effect on soil evaporation | $\mu$ | 2.77 | |
| | Aerodynamic ET exponent | $\beta_a$ | $\frac{4.80}{1+e^{-11.54*(\overline{E}_p-2.65)}}+0.20$ * | |
| | Radiative ET exponent | $\beta_r$ | $\frac{-4.80}{1+e^{-6.84*(\overline{E}_p-3.76)}}+5.00$ * | |

* This reference parameter is determined from the CGIAR-CSI PET dataset.
† This reference parameter is determined from the ISRIC-WISE soil dataset.

Table 2. Root mean square error (RMSE) ($m^3 m^{-3}$) of the locally calibrated and global applications of the EMT+VS model.

| | Tarrawarra | Satellite Station | Cache la Poudre | Nerrigundah | Reynolds Creek | Tibet |
|---|---|---|---|---|---|---|
| Calibrated | 0.028 | 0.048 | 0.030 | 0.048 | 0.055 | 0.053 |
| Global | 0.032 | 0.050 | 0.031 | 0.050 | 0.067 | 0.060 |

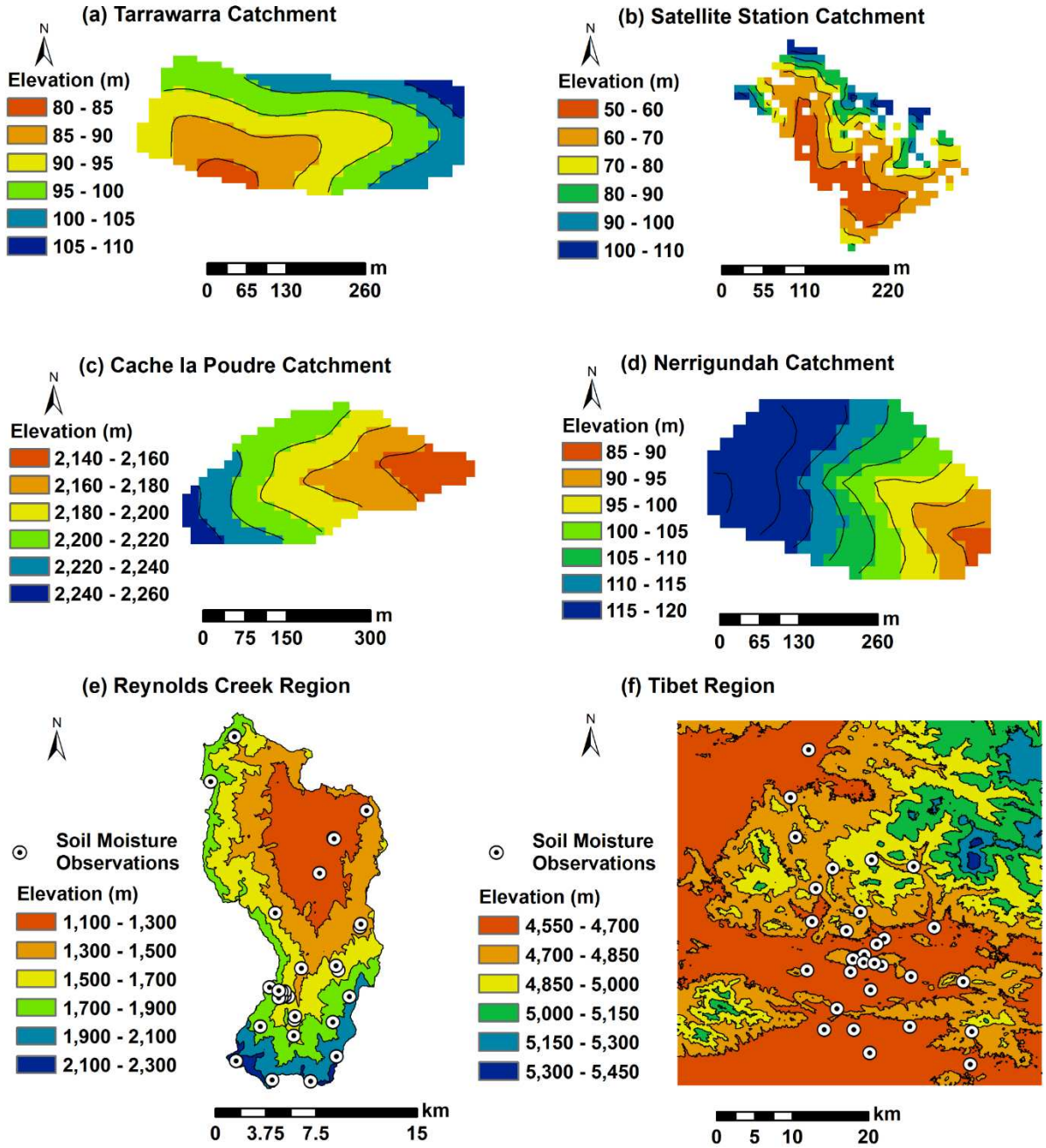


Figure 1. Elevation maps of the four small catchments (a) Tarrawarra, (b) Satellite Station, (c) Cache la Poudre, and (d) Nerrigundah and two large regions (e) Reynolds Creek, and (f) Tibet used for EMT+VS model evaluation. For the catchments, soil moisture observations are available at nearly every elevation grid cell. For the regions, the symbols indicate the locations with soil moisture observations.

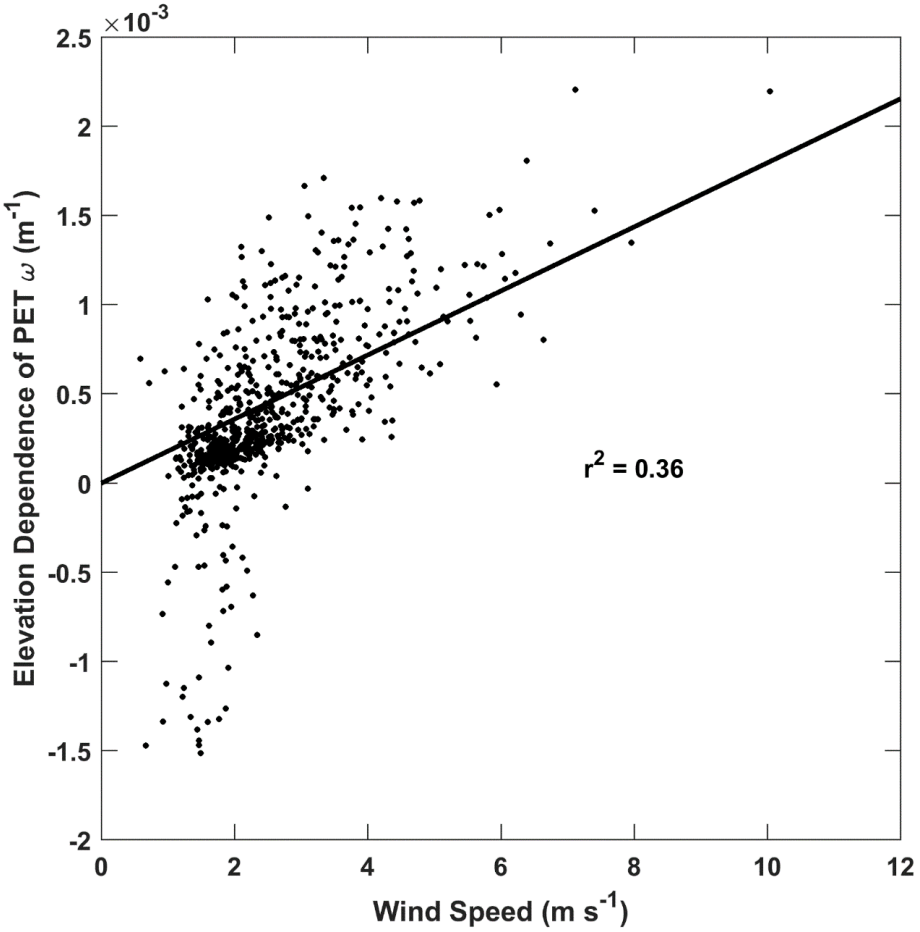


Figure 2. Daily $\omega$ values estimated from potential ET and elevation data at Reynolds Creek plotted as a function of daily wind speed. The fitted relationship between those two variables is also shown with the coefficient of determination $r^2$.

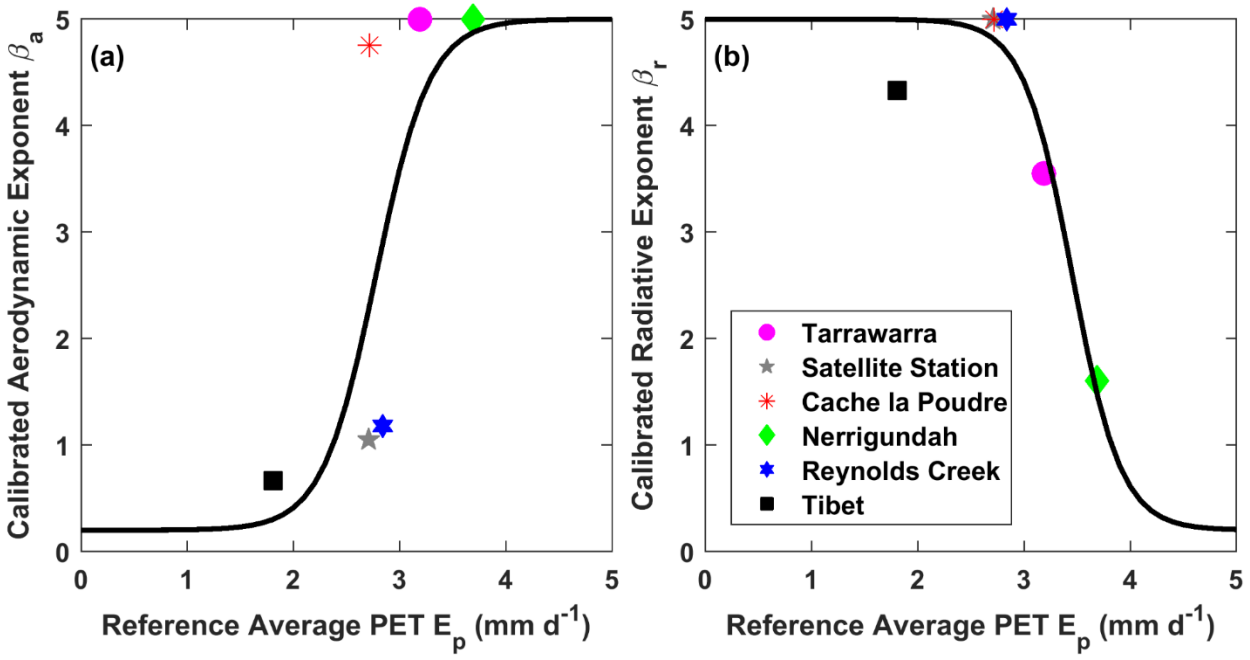


Figure 3. Calibrated (a) $\beta_a$ and (b) $\beta_r$ values plotted as a function of the reference $\overline{E}_p$ values for each study site. The fitted generalized logistic function is also shown (solid line).

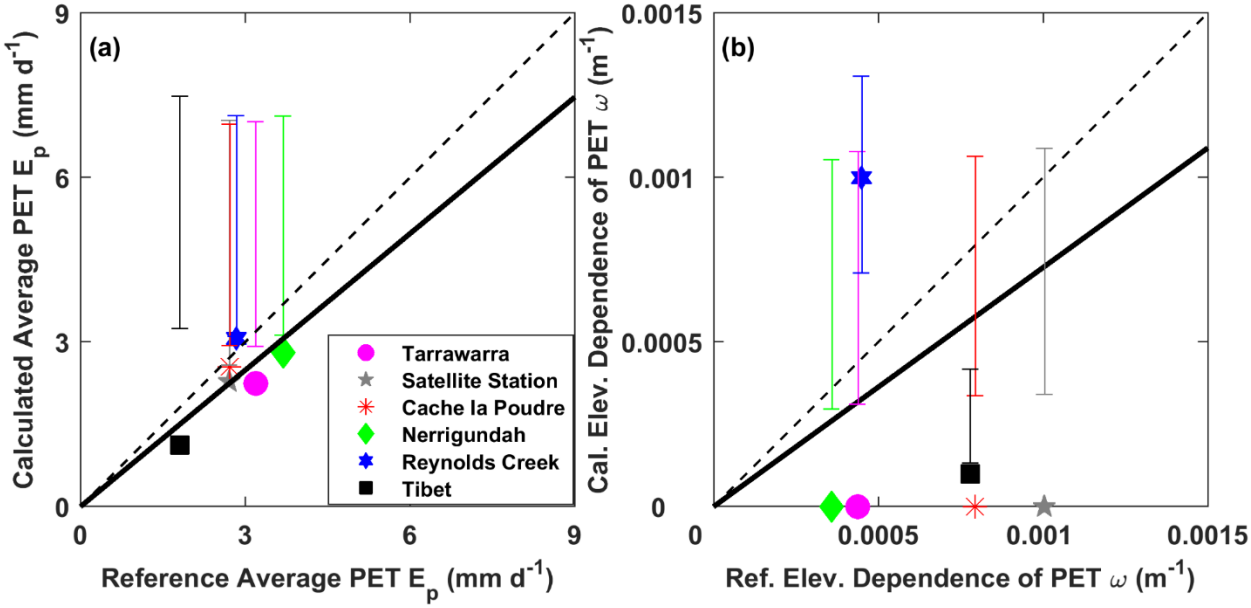


Figure 4. Calibrated values for climate parameters (a) $\overline{E}_p$ and (b) $\omega$ plotted against their reference values for the six study sites with vertical error bars showing the interquartile ranges (IQRs) from Generalized Likelihood Uncertainty Estimation (GLUE). 1:1 (dashed) and regression (solid) lines are also shown.

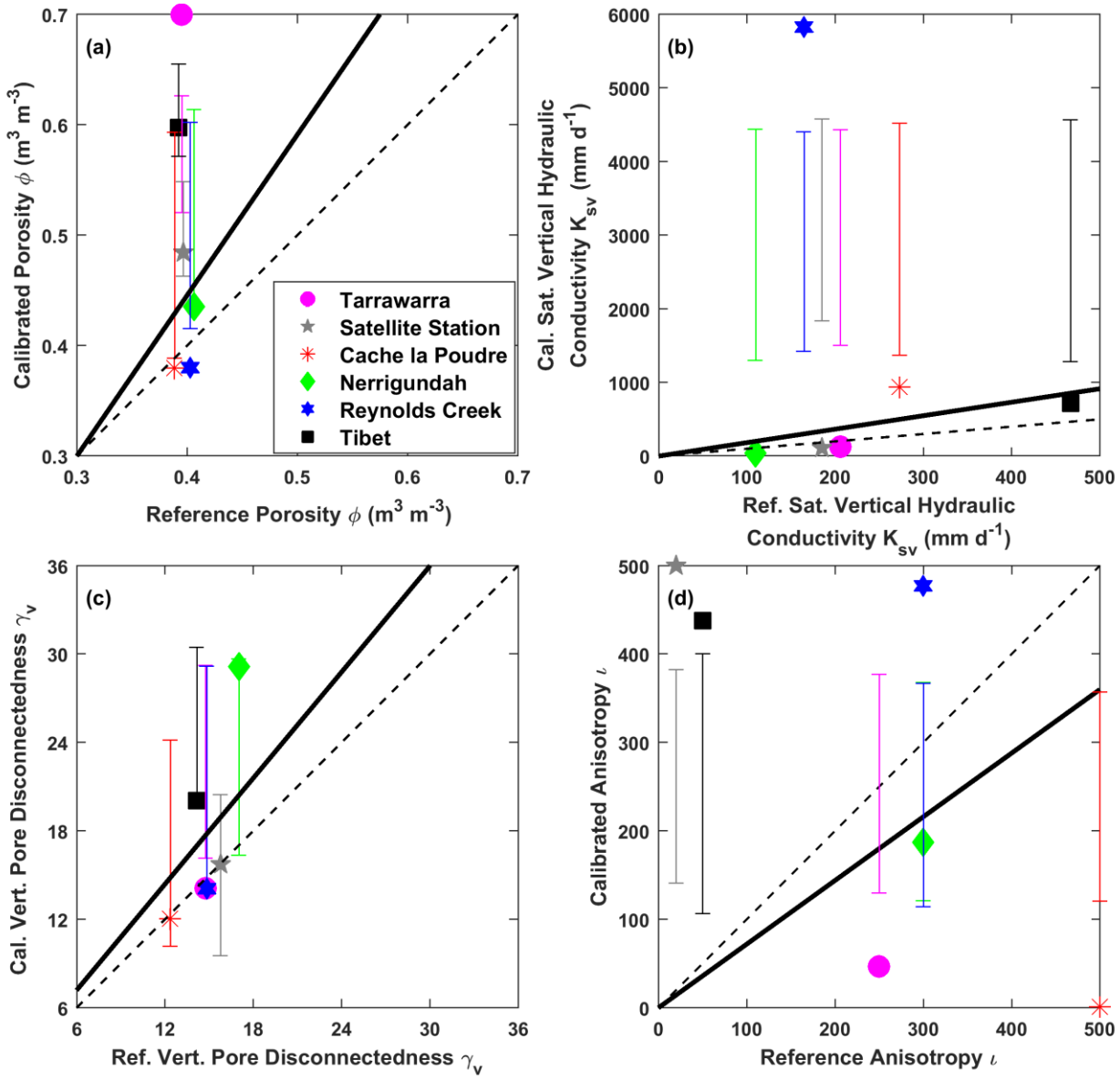


Figure 5. Calibrated values for soil parameters (a) $\phi$, (b) $K_{s,v}$, (c) $\gamma_v$, and (d) $\iota$ plotted against their reference values for the six study sites with vertical error bars showing the interquartile ranges (IQRs) from Generalized Likelihood Uncertainty Estimation (GLUE). 1:1 (dashed) and regression (solid) lines are also shown.

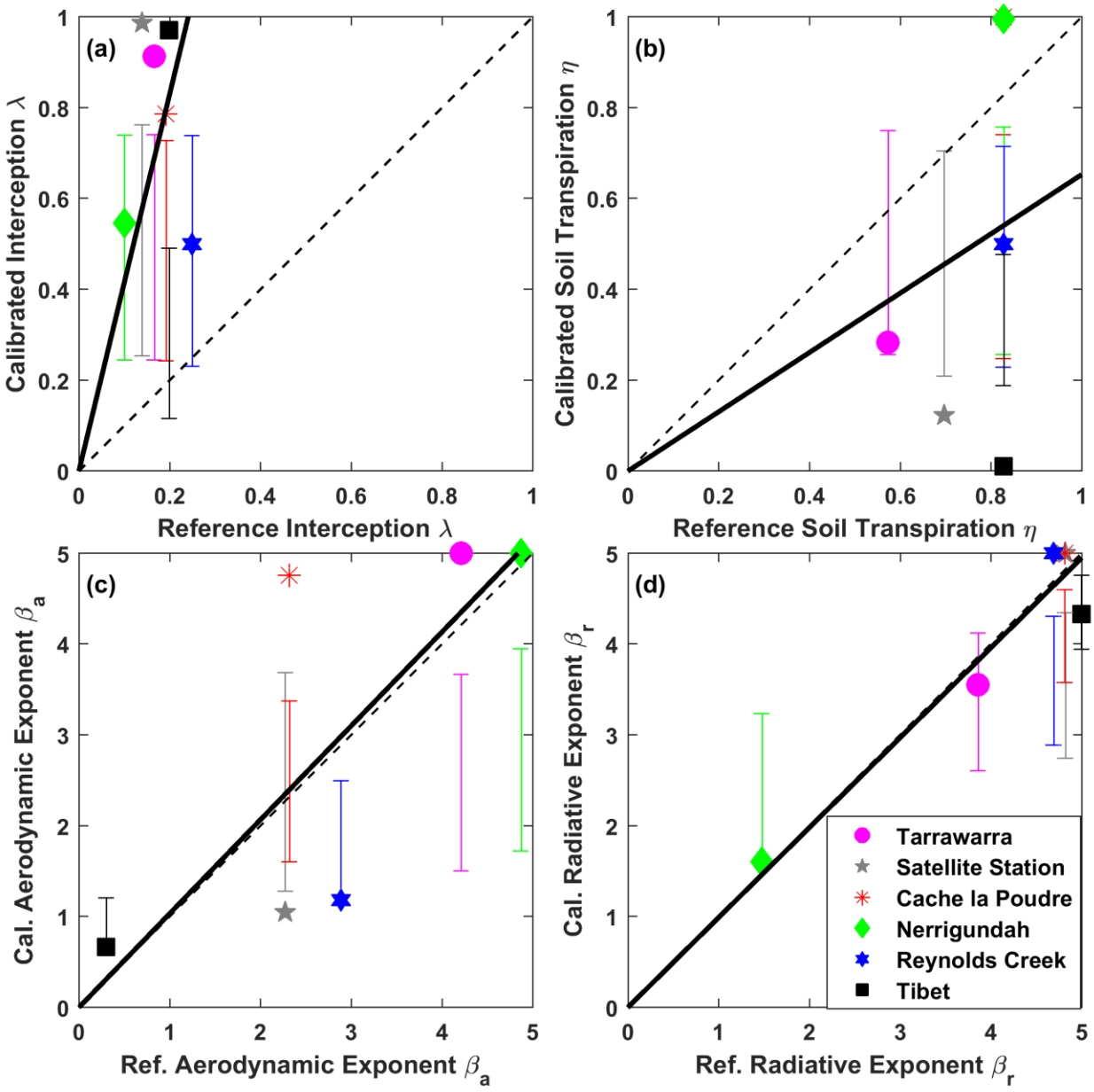


Figure 6. Calibrated values for vegetation parameters (a) $\lambda$, (b) $\eta$, (c) $\beta_a$, and (d) $\beta_r$ plotted against their reference values for the six study sites with vertical error bars showing interquartile ranges (IQRs) from Generalized Likelihood Uncertainty Estimation (GLUE). 1:1 (dashed) and regression (solid) lines are also shown.

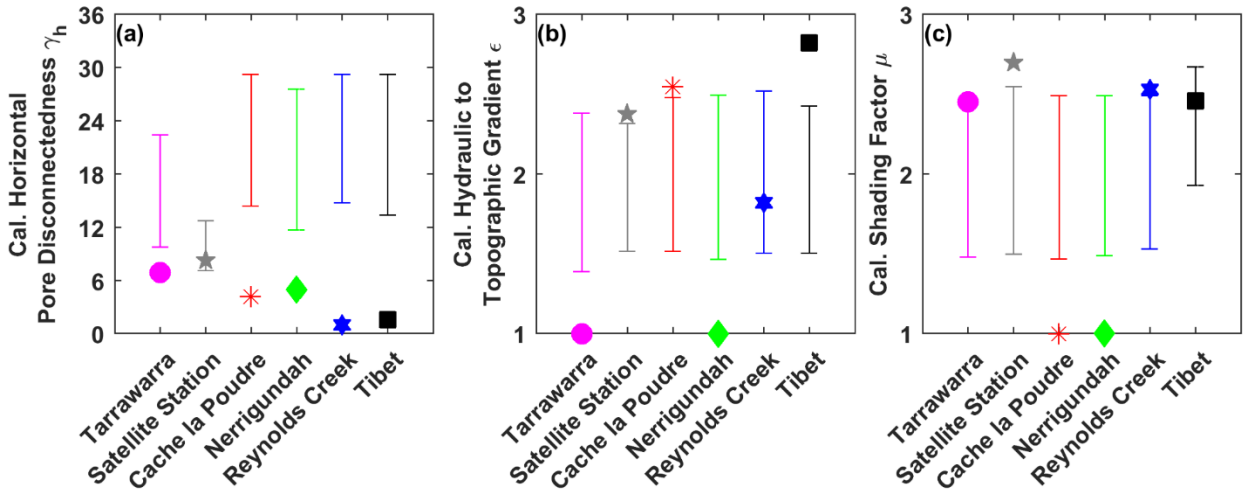


Figure 7. Calibrated values for (a) $\gamma_h$, (b) $\varepsilon$, and (c) $\mu$ at the six study sites with vertical error bars showing the interquartile ranges (IQRs) from Generalized Likelihood Uncertainty Estimation (GLUE).

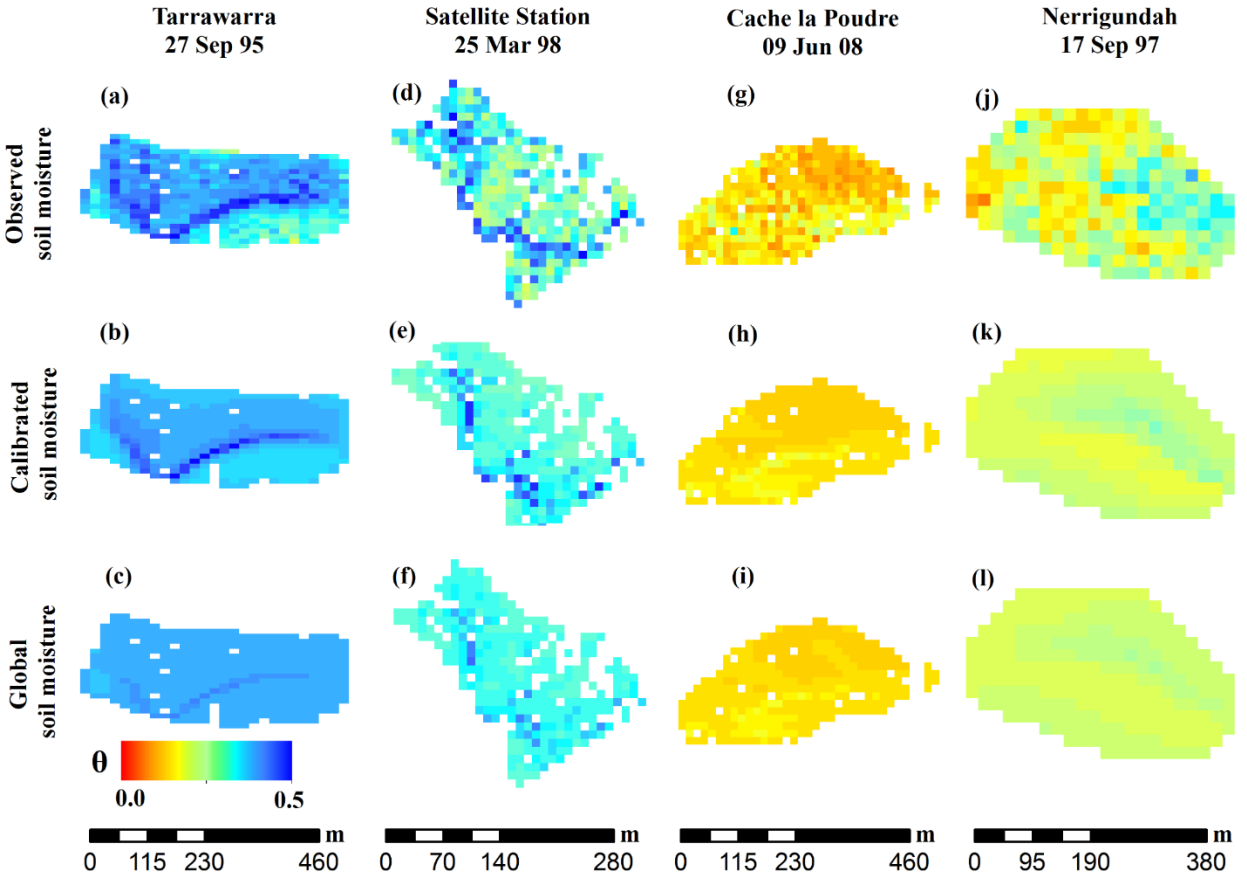


Figure 8. Maps of the soil moisture ($\theta$, $m^3\ m^{-3}$) patterns from the observations (top), calibrated EMT+VS model (middle), and global EMT+VS model (bottom) for example dates at the four catchments (a-c) Tarrawarra, (d-f) Satellite Station, (g-i) Cache la Poudre, and (j-l) Nerrigundah. The global model uses the recommended parameters.

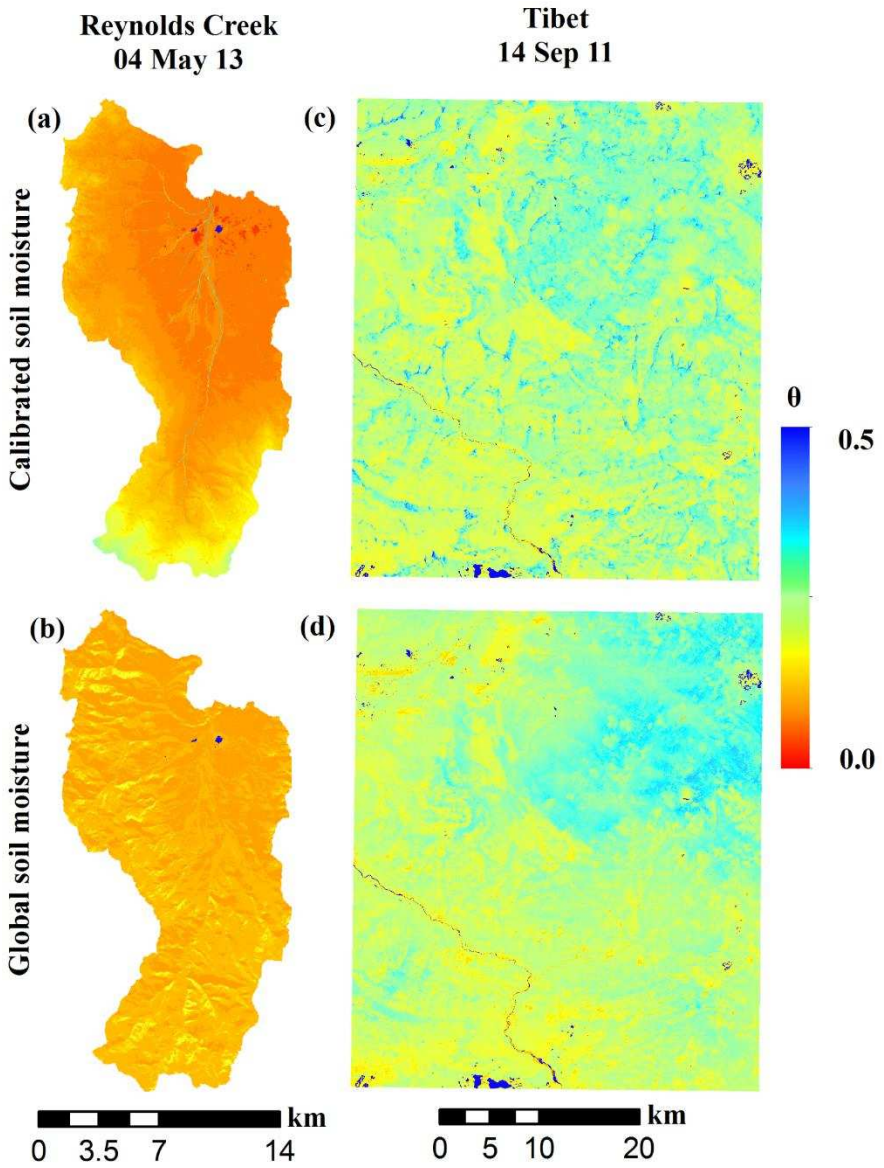


Figure 9. Maps of the calibrated (top) and global (bottom) EMT+VS model soil moisture ($\theta$, $m^3$ $m^{-3}$) patterns for example dates at the two regions (a-b) Reynolds Creek and (c-d) Tibet. The global model uses the recommended parameters.

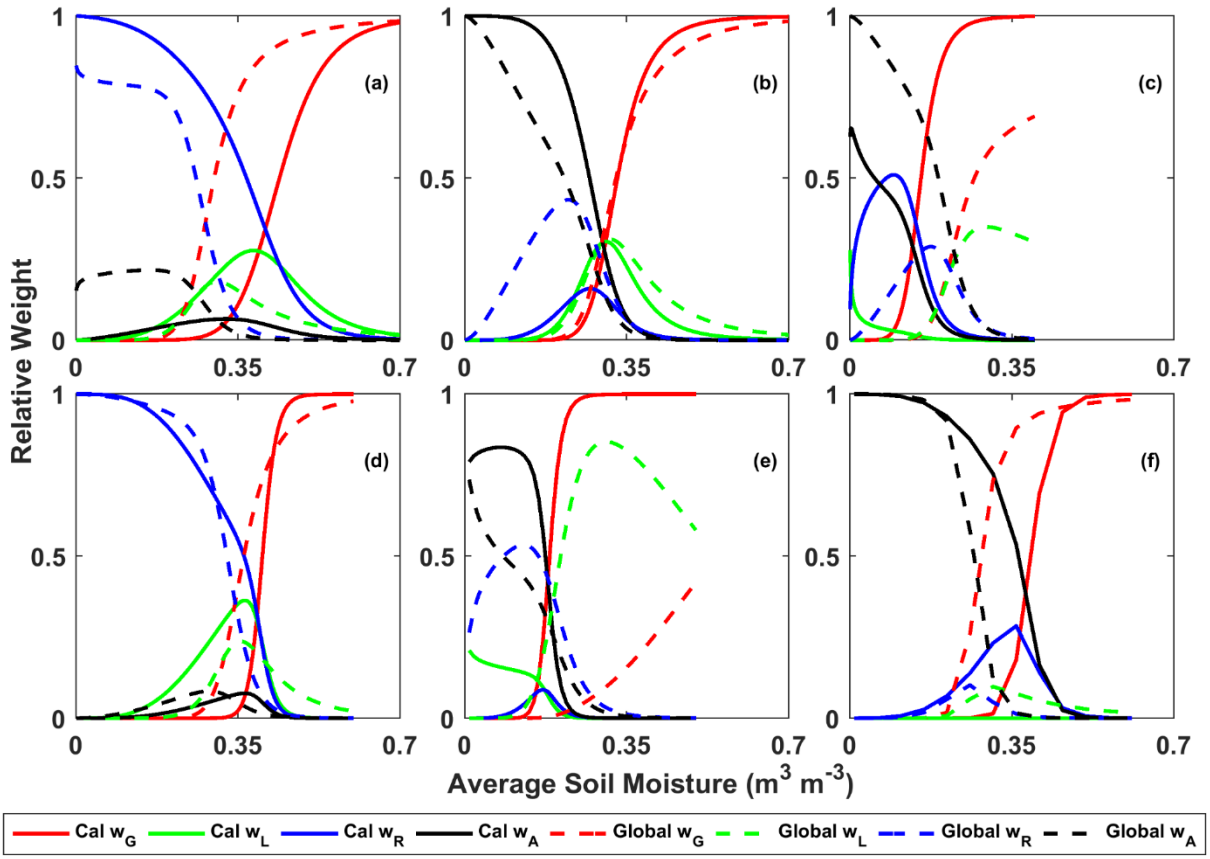


Figure 10. Locally calibrated and global relative weights for the six study sites (a) Tarrawarra, (b) Satellite Station, (c) Cache la Poudre, (d) Nerrigundah, (e) Reynolds Creek, and (f) Tibet. The weights for each site are shown for the range of average soil moisture values included in the associated soil moisture observations.

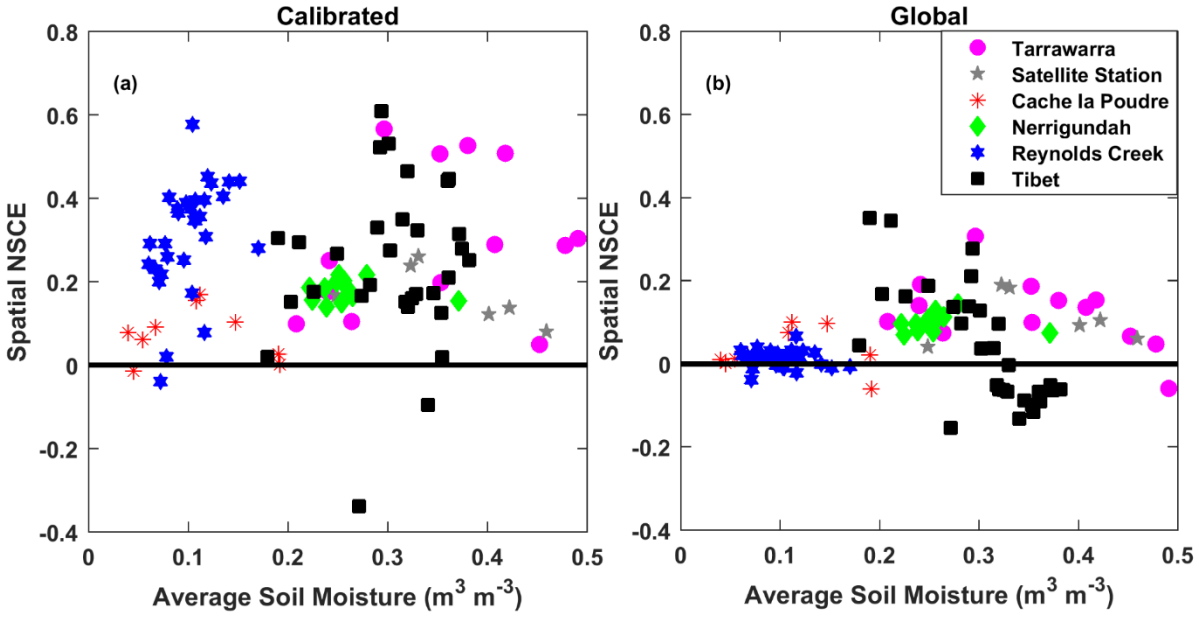


Figure 11. Spatial Nash-Sutcliffe Coefficient of Efficiency (NSCE) plotted as a function of spatial average soil moisture for the (a) calibrated and (b) global models at the six study sites.

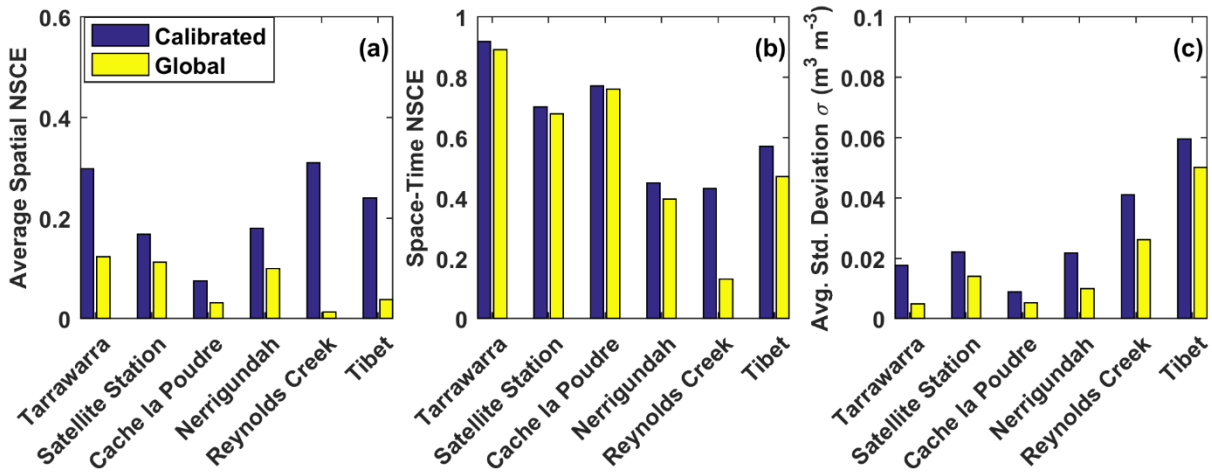


Figure 12. Comparison of (a) average spatial Nash-Sutcliffe Coefficient of Efficiency (NSCE), (b) space-time NSCE, and (c) average spatial standard deviations for the locally calibrated and global EMT+VS models.

# REFERENCES


Alburn, N. E., Niemann, J. D., & Elhaddad, A. 2015. Evaluation of a surface energy balance method based on optical and thermal satellite imagery to estimate root-zone soil moisture. Hydrological Processes, 29(26), 5354-5368. doi: 10.1002/hyp.10562

Bartalis, Z., Wagner, W., Naeimi, V., Hasenauer, S., Scipal, K., Bonekamp, H., et al. 2007. Initial soil moisture retrievals from the METOP-A Advanced Scatterometer (ASCAT). Geophysical Research Letters, 34(20). doi: 10.1029/2007gl091088

Batjes, N. H. (2015). World soil property estimates for broad-scale modelling (WISE30sec). Wageningen, The Netherlands: ISRIC - World Soil Information.

Beven, K., & Binley, A. 1992. The future of distributed models - Model calibration and uncertainty prediction. Hydrological Processes, 6(3), 279-298. doi: 10.1002/hyp.3360060305

Bolten, J. D., Crow, W. T., Zhan, X. W., Jackson, T. J., & Reynolds, C. A. 2010. Evaluating the Utility of Remotely Sensed Soil Moisture Retrievals for Operational Agricultural Drought Monitoring. Ieee Journal of Selected Topics in Applied Earth Observations and Remote Sensing, 3(1), 57-66. doi: 10.1109/jstars.2009.2037163

Bonan, G. B. 1998. The land surface climatology of the NCAR Land Surface Model coupled to the NCAR Community Climate Model. Journal of Climate, 11(6), 1307-1326. doi: 10.1175/1520-0442(1998)011<1307:tlscot>2.0.co;2

Bontemps, S., Defourny, P., Bogaert, E., Arino, O., Kalogirou, V., & Perez, J. 2011. GLOBCOVER 2009 - Products description and validation report. ESA and UCLouvain.

Busch, F. A., Niemann, J. D., & Coleman, M. 2012. Evaluation of an empirical orthogonal function-based method to downscale soil moisture patterns based on topographical attributes. Hydrological Processes, 26(18), 2696-2709. doi: 10.1002/hyp.8363

Campbell, G. S. 1974. Simple method for determining unsaturated conductivity from moisture retention data. Soil Science, 117(6), 311-314.

Carlson, T. 2007. An overview of the "triangle method" for estimating surface evapotranspiration and soil moisture from satellite imagery. Sensors, 7(8), 1612-1629. doi: 10.3390/s7081612

Carsel, R. F., & Parrish, R. S. 1988. Developing joint probability distributions of soil water retention characteristics. Water Resources Research, 24(5), 755-769. doi: 10.1029/WR024i005p00755

Chauhan, N. S., Miller, S., & Ardanuy, P. 2003. Spaceborne soil moisture estimation at high resolution: a microwave-optical/IR synergistic approach. International Journal of Remote Sensing, 24(22), 4599-4622. doi: 10.1080/0143116031000156837

Coleman, M. L., & Niemann, J. D. 2012. An evaluation of nonlinear methods for estimating catchment-scale soil moisture patterns based on topographic attributes. Journal of Hydroinformatics, 14(3), 800-814. doi: 10.2166/hydro.2012.145

Coleman, M. L., & Niemann, J. D. 2013. Controls on topographic dependence and temporal instability in catchment-scale soil moisture patterns. Water Resources Research, 49(3), 1625-1642. doi: 10.1002/wrcr.20159

Colliander, A., Jackson, T. J., Bindlish, R., Chan, S., Das, N., Kim, S. B., et al. 2017. Validation of SMAP surface soil moisture products with core validation sites. Remote Sensing of Environment, 191, 215-231. doi: 10.1016/j.rse.2017.01.021

Cosby, B. J., Hornberger, G. M., Clapp, R. B., & Ginn, T. R. 1984. A statistical exploration of the relationships of soil moisture characteristics to the physical properties of soils. Water Resources Research, 20(6), 682-690. doi: 10.1029/WR020i006p00682

Cowley, G. S., Niemann, J. D., Green, T. R., Seyfried, M. S., Jones, A. S., & Grazaitis, P. J. 2017. Impacts of precipitation and potential evapotranspiration patterns on downscaling soil moisture in regions with large topographic relief. Water Resources Research. doi: 10.1002/2016wr019907

Das, N. N., Entekhabi, D., & Njoku, E. G. 2011. An Algorithm for Merging SMAP Radiometer and Radar Data for High-Resolution Soil-Moisture Retrieval. Ieee Transactions on Geoscience and Remote Sensing, 49(5), 1504-1512. doi: 10.1109/tgrs.2010.2089526

Das, N. N., Entekhabi, D., Njoku, E. G., Shi, J., Johnson, J. T., & Colliander, A. 2014. Tests of the SMAP Combined Radar and Radiometer Algorithm Using Airborne Field Campaign Observations and Simulated Data. Ieee Transactions on Geoscience and Remote Sensing, 52(4), 2018-2028. doi: 10.1109/tgrs.2013.2257605

De Lannoy, G. J. M., Reichle, R. H., Houser, P. R., Pauwels, V. R. N., & Verhoest, N. E. C. 2007. Correcting for forecast bias in soil moisture assimilation with the ensemble Kalman filter. Water Resources Research, 43(9). doi: 10.1029/2006wr005449

Delworth, T., & Manabe, S. 1989. The Influence of Soil Wetness on near-Surface Atmospheric Variability. Journal of Climate, 2(12), 1447-1462. doi: Doi 10.1175/1520-0442(1989)002<1447:Tioswo>2.0.Co;2

Dile, Y. T., & Srinivasan, R. 2014. Evaluation of CFSR climate data for hydrologic prediction in data-scarce watersheds: an application in the Blue Nile River Basin. Journal of the American Water Resources Association, 50(5), 1226-1241. doi: 10.1111/jawr.12182

Dingman, S. L. 2015. Physical Hydrology. 3rd ed. Waveland Press, Inc Long Grove, Illinois.

Dirmeyer, P. A. 1999. Assessing GCM sensitivity to soil wetness using GSWP data. Journal of the Meteorological Society of Japan, 77(1B), 367-385.

Droesen, J. 2016. Downscaling soil moisture using topography: The evaluation and optimisation of a downscaling approach. M.S. Thesis, Wageningen University and Research Centre, Wageningen, The Netherlands.

Ek, M. B., Mitchell, K. E., Lin, Y., Rogers, E., Grunmann, P., Koren, V., et al. 2003. Implementation of Noah land surface model advances in the National Centers for Environmental Prediction operational mesoscale Eta model. Journal of Geophysical Research-Atmospheres, 108(D22). doi: 10.1029/2002jd003296

Entekhabi, D., Njoku, E. G., O'Neill, P. E., Kellogg, K. H., Crow, W. T., Edelstein, W. N., et al. 2010. The Soil Moisture Active Passive (SMAP) Mission. Proceedings of the Ieee, 98(5), 704-716. doi: 10.1109/jproc.2010.2043918

Ershadi, A., McCabe, M. F., Evans, J. P., Chaney, N. W., & Wood, E. F. 2014. Multi-site evaluation of terrestrial evaporation models using FLUXNET data. Agricultural and Forest Meteorology, 187, 46-61. doi: 10.1016/j.agrformet.2013.11.008

Famiglietti, J., & Wood, E. 1994. Multiscale modeling of spatially-variable water and energy-balance processes. Water Resources Research, 30(11), 3061-3078. doi: 10.1029/94wr01498

FAO, IIASA, ISRIC, ISS-CAS, & JRC. (2012). Harmonized World Soil Database (version 1.2). Rome, Italy and Laxenburg, Austria: FAO and IIASA.

Flores, A. N., Entekhabi, D., & Bras, R. L. 2014. Application of a hillslope-scale soil moisture data assimilation system to military trafficability assessment. Journal of Terramechanics, 51, 53-66. doi: 10.1016/j.jterra.2013.11.004

Friedl, M. A., Sulla-Menashe, D., Tan, B., Schneider, A., Ramankutty, N., Sibley, A., et al. 2010. MODIS Collection 5 global land cover: Algorithm refinements and characterization of new datasets. Remote Sensing of Environment, 114(1), 168-182. doi: 10.1016/j.rse.2009.08.016

Fuka, D. R., Walter, M. T., MacAlister, C., Degaetano, A. T., Steenhuis, T. S., & Easton, Z. M. 2014. Using the Climate Forecast System Reanalysis as weather input data for watershed models. Hydrological Processes, 28(22), 5613-5623. doi: 10.1002/hyp.10073

Galdos, F. V., Alvarez, C., Garcia, A., & Revilla, J. A. 2012. Estimated distributed rainfall interception using a simple conceptual model and Moderate Resolution Imaging Spectroradiometer (MODIS). Journal of Hydrology, 468, 213-228. doi: 10.1016/j.jhydrol.2012.08.043

Green, T. R., & Erskine, R. H. 2004. Measurement, scaling, and topographic analyses of spatial crop yield and soil water content. Hydrological Processes, 18(8), 1447-1465. doi: 10.1002/hyp.1422

Grekousis, G., Mountrakis, G., & Kavouras, M. 2015. An overview of 21 global and 43 regional land-cover mapping products. International Journal of Remote Sensing, 36(21), 5309-5335. doi: 10.1080/01431161.2015.1093195

Hanson, C. L. 1989. Prediction of class A pan evaporation in Southwest Idaho. Journal of Irrigation and Drainage Engineering-Asce, 115(2), 166-171.

Hanson, C. L. 2001. Long-term precipitation database, Reynolds Creek Experimental Watershed, Idaho, United States. Water Resources Research, 37(11), 2831-2834. doi: 10.1029/2001wr000415

Hanson, C. L., Marks, D., & Van Vactor, S. S. 2001. Long-term climate database, Reynolds Creek Experimental Watershed, Idaho, United States. Water Resources Research, 37(11), 2839-2841. doi: 10.1029/2001wr000417

Hoehn, D. C., Niemann, J. D., Green, T. R., Jones, A. S., & Grazaitis, P. J. 2017. Downscaling soil moisture over regions that include multiple coarse-resolution grid cells. Remote Sensing of Environment, 199, 187-200. doi: https://doi.org/10.1016/j.rse.2017.07.021

Horn, R., & Fleige, H. 2003. A method for assessing the impact of load on mechanical stability and on physical properties of soils. Soil & Tillage Research, 73(1-2), 89-99. doi: 10.1016/s0167-1987(03)00102-8

Houser, P. R., Shuttleworth, W. J., Famiglietti, J. S., Gupta, H. V., Syed, K. H., & Goodrich, D. C. 1998. Integration of soil moisture remote sensing and hydrologic modeling using data assimilation. Water Resources Research, 34(12), 3405-3420. doi: 10.1029/1998wr900001

Huete, A. R. 1988. A soil-adjusted vegetation index (SAVI). Remote Sensing of Environment, 25(3), 295-309. doi: 10.1016/0034-4257(88)90106-x

Huisman, J. A., Sperl, C., Bouten, W., & Verstraten, J. M. 2001. Soil water content measurements at different scales: accuracy of time domain reflectometry and ground-penetrating radar. Journal of Hydrology, 245(1-4), 48-58. doi: 10.1016/s0022-1694(01)00336-5

Ines, A. V. M., Mohanty, B. P., & Shin, Y. 2013. An unmixing algorithm for remotely sensed soil moisture. Water Resources Research, 49(1), 408-425. doi: 10.1029/2012wr012379

Jackson, R. B., Canadell, J., Ehleringer, J. R., Mooney, H. A., Sala, O. E., & Schulze, E. D. 1996. A global analysis of root distributions for terrestrial biomes. Oecologia, 108(3), 389-411. doi: 10.1007/bf00333714

Jackson, R. B., Sperry, J. S., & Dawson, T. E. 2000. Root water uptake and transport: using physiological processes in global predictions. Trends in Plant Science, 5(11), 482-488. doi: 10.1016/s1360-1385(00)01766-0

Jackson, T., O'Neill, P., Njoku, E., Chan, S., Bindlish, R., Colliander, A., et al. 2016. Soil Moisture Active Passive (SMAP) Project Calibration and Validation for the L2/3_SM_P Version 3 Data Products SMAP Project.

Jarvis, N. J. 1989. A simple empirical model of root water uptake. Journal of Hydrology, 107(1-4), 57-72. doi: 10.1016/0022-1694(89)90050-4

Kaheil, Y. H., Gill, M. K., McKee, M., Bastidas, L. A., & Rosero, E. 2008. Downscaling and assimilation of surface soil moisture using ground truth measurements. Ieee Transactions on Geoscience and Remote Sensing, 46(5), 1375-1384. doi: 10.1109/tgrs.2008.916086

Kerr, Y. H., Waldteufel, P., Wigneron, J. P., Delwart, S., Cabot, F., Boutin, J., et al. 2010. The SMOS Mission: New Tool for Monitoring Key Elements of the Global Water Cycle. Proceedings of the Ieee, 98(5), 666-687. doi: 10.1109/jproc.2010.2043032

Kim, G., & Barros, A. P. 2002. Downscaling of remotely sensed soil moisture with a modified fractal interpolation method using contraction mapping and ancillary data. Remote Sensing of Environment, 83(3), 400-413. doi: 10.1016/s0034-4257(02)00044-5

Kim, J., & Hogue, T. S. 2012. Improving Spatial Soil Moisture Representation Through Integration of AMSR-E and MODIS Products. Ieee Transactions on Geoscience and Remote Sensing, 50(2), 446-460. doi: 10.1109/tgrs.2011.2161318

Koster, R. D., & Suarez, M. J. 2003. Impact of land surface initialization on seasonal precipitation and temperature prediction. Journal of Hydrometeorology, 4(2), 408-423. doi: 10.1175/1525-7541(2003)4<408:iolsio>2.0.co;2

Kumar, S. V., Peters-Lidard, C. D., Mocko, D., Reichle, R., Liu, Y., Arsenault, K. R., et al. 2014. Assimilation of Remotely Sensed Soil Moisture and Snow Depth Retrievals for Drought Estimation. Journal of Hydrometeorology, 15(6), 2446-2469. doi: 10.1175/jhm-d-13-0132.1

Kumar, S. V., Peters-Lidard, C. D., Tian, Y., Houser, P. R., Geiger, J., Olden, S., et al. 2006. Land information system: An interoperable framework for high resolution land surface modeling. Environmental Modelling & Software, 21(10), 1402-1415. doi: 10.1016/j.envsoft.2005.07.004

Laio, F., Porporato, A., Ridolfi, L., & Rodriguez-Iturbe, I. 2001. Plants in water-controlled ecosystems: active role in hydrologic processes and response to water stress - II. Probabilistic soil moisture dynamics. Advances in Water Resources, 24(7), 707-723. doi: 10.1016/s0309-1708(01)00005-7

Latham, J., Cumani, R., Rosati, I., & Bloise, M. 2014. Global land cover share (GLC-SHARE) database beta-release version 1.0-2014. FAO: Rome, Italy.

Lehner, B., Verdin, K., & Jarvis, A. 2008. New global hydrography derived from spaceborne elevation data. Eos, Transaction, AGU, 89(10), 93-94.

Li, L., Gaiser, P. W., Gao, B. C., Bevilacqua, R. M., Jackson, T. J., Njoku, E. G., et al. 2010. WindSat Global Soil Moisture Retrieval and Validation. Ieee Transactions on Geoscience and Remote Sensing, 48(5), 2224-2241. doi: 10.1109/tgrs.2009.2037749

Liang, X., Lettenmaier, D. P., & Wood, E. F. 1996. One-dimensional statistical dynamic representation of subgrid spatial variability of precipitation in the two-layer variable infiltration capacity model. Journal of Geophysical Research: Atmospheres, 101(D16), 21403-21422. doi: 10.1029/96jd01448

Loveland, T. R., & Belward, A. S. 1997. The IGBP-DIS global 1 km land cover data set, DISCover: first results. International Journal of Remote Sensing, 18(15), 3291-3295.

Loveland, T. R., Reed, B. C., Brown, J. F., Ohlen, D. O., Zhu, Z., Yang, L., et al. 2000. Development of a global land cover characteristics database and IGBP DISCover from 1 km AVHRR data. International Journal of Remote Sensing, 21(6-7), 1303-1330. doi: 10.1080/014311600210191

Lowry, W. 1959. Lowry, W. P. (1959). The falling rate phase of evaporative soil moisture loss: A critical evaluation. Bulletin of the American Meteorological Society, 40(12), 605-608.

Maidment, D. R. 1993. Handbook of hydrology Vol. 1. McGraw-Hill New York.

Mascaro, G., Vivoni, E. R., & Deidda, R. 2010. Downscaling soil moisture in the southern Great Plains through a calibrated multifractal model for land surface modeling applications. Water Resources Research, 46. doi: 10.1029/2009wr008855

Merlin, O., Escorihuela, M. J., Mayoral, M. A., Hagolle, O., Al Bitar, A., & Kerr, Y. 2013. Self-calibrated evaporation-based disaggregation of SMOS soil moisture: An evaluation study at 3 km and 100 m resolution in Catalunya, Spain. Remote Sensing of Environment, 130, 25-38. doi: 10.1016/j.rse.2012.11.008

Mu, Q. Z., Zhao, M. S., & Running, S. W. 2011. Improvements to a MODIS global terrestrial evapotranspiration algorithm. Remote Sensing of Environment, 115(8), 1781-1800. doi: 10.1016/j.rse.2011.02.019

Nash, J. E., & Sutcliffe, J. V. 1970. River flow forecasting through conceptual models part I - a discussion of principles. Journal of Hydrology, 10, 282-290.

Nelson, R. M. 2001. Water Relations of Forest Fuels. Academic Press San Diego, CA.

Njoku, E. G., Jackson, T. J., Lakshmi, V., Chan, T. K., & Nghiem, S. V. 2003. Soil moisture retrieval from AMSR-E. Ieee Transactions on Geoscience and Remote Sensing, 41(2), 215-229. doi: 10.1109/tgrs.2002.808243

Parinussa, R. M., Holmes, T. R. H., Wanders, N., Dorigo, W. A., & de Jeu, R. A. M. 2015. A Preliminary Study toward Consistent Soil Moisture from AMSR2. Journal of Hydrometeorology, 16(2), 932-947. doi: 10.1175/jhm-d-13-0200.1

Pellenq, J., Kalma, J., Boulet, G., Saulnier, G. M., Wooldridge, S., Kerr, Y., et al. 2003. A disaggregation scheme for soil moisture based on topography and soil depth. Journal of Hydrology, 276(1-4), 112-127. doi: 10.1016/s0022-1694(03)00066-0

Peng, J., Loew, A., Merlin, O., & Verhoest, N. 2017. A review of spatial downscaling of satellite remotely sensed soil moisture. Reviews of Geophysics, 55. doi: 10.1002/2016RG000543

Perry, M. A., & Niemann, J. D. 2007. Analysis and estimation of soil moisture at the catchment scale using EOFs. Journal of Hydrology, 334(3-4), 388-404. doi: 10.1016/j.jhydrol.2006.10.014

Peterson, T. C., & Vose, R. S. 1997. An overview of the global historical climatology network temperature database. Bulletin of the American Meteorological Society, 78(12), 2837-2849. doi: 10.1175/1520-0477(1997)078<2837:aootgh>2.0.co;2

Piles, M., Petropoulos, G. P., Sanchez, N., Gonzalez-Zamora, A., & Ireland, G. 2016. Towards improved spatio-temporal resolution soil moisture retrievals from the synergy of SMOS and MSG SEVIRI spaceborne observations. Remote Sensing of Environment, 180, 403-417. doi: 10.1016/j.rse.2016.02.048

Porporato, A., Daly, E., & Rodriguez-Iturbe, I. 2004. Soil water balance and ecosystem response to climate change. American Naturalist, 164(5), 625-632. doi: 10.1086/424970

Priestley, C. H. B., & Taylor, R. J. 1972. Assessment of surface heat flux and evaporation using large-scale parameters. Monthly Weather Review, 100(2), 81-+. doi: 10.1175/1520-0493(1972)100<0081:otaosh>2.3.co;2

Ranney, K. J., Niemann, J. D., Lehman, B. M., Green, T. R., & Jones, A. S. 2015. A method to downscale soil moisture to fine resolutions using topographic, vegetation, and soil data. Advances in Water Resources, 76, 81-96. doi: 10.1016/j.advwatres.2014.12.003

Rosero, E., Yang, Z. L., Wagener, T., Gulden, L. E., Yatheendradas, S., & Niu, G. Y. 2010. Quantifying parameter sensitivity, interaction, and transferability in hydrologically enhanced versions of the Noah land surface model over transition zones during the warm season. Journal of Geophysical Research-Atmospheres, 115. doi: 10.1029/2009jd012035

Saha, S., Moorthi, S., Pan, H. L., Wu, X. R., Wang, J. D., Nadiga, S., et al. 2010. The NCEP Climate Forecast System Reanalysis. Bulletin of the American Meteorological Society, 91(8), 1015-1057. doi: 10.1175/2010bams3001.1

Sahoo, A. K., De Lannoy, G. J. M., Reichle, R. H., & Houser, P. R. 2013. Assimilation and downscaling of satellite observed soil moisture over the Little River Experimental Watershed in Georgia, USA. Advances in Water Resources, 52, 19-33. doi: 10.1016/j.advwatres.2012.08.007

Sanchez, P. A., Ahamed, S., Carre, F., Hartemink, A. E., Hempel, J., Huising, J., et al. 2009. Digital Soil Map of the World. Science, 325(5941), 680-681. doi: 10.1126/science.1175084

Saxton, K. E., & Rawls, W. J. 2006. Soil water characteristic estimates by texture and organic matter for hydrologic solutions. Soil Science Society of America Journal, 70(5), 1569-1578. doi: 10.2136/sssaj2005.0117

Schenk, H. J., & Jackson, R. B. 2002. The global biogeography of roots. Ecological Monographs, 72(3), 311-328. doi: 10.1890/0012-9615(2002)072[0311:tgbor]2.0.co;2

Sellers, P. J., Mintz, Y., Sud, Y. C., & Dalcher, A. 1986. A simple biosphere model (SiB) for use within general circulation models. Journal of the Atmospheric Sciences, 43(6), 505-531. doi: 10.1175/1520-0469(1986)043<0505:asbmfu>2.0.co;2

Seuffert, G., Gross, P., Simmer, C., & Wood, E. F. 2002. The influence of hydrologic modeling on the predicted local weather: Two-way coupling of a mesoscale weather prediction model and a land surface hydrologic model. Journal of Hydrometeorology, 3(5), 505-523. doi: 10.1175/1525-7541(2002)003<0505:tiohmo>2.0.co;2

Seyfried, M., Harris, R., Marks, D., & Jacob, B. 2001. Geographic database, Reynolds Creek Experimental Watershed, Idaho, United States. Water Resources Research, 37(11), 2825-2829. doi: 10.1029/2001wr000414

Seyfried, M. S., Grant, L. E., Du, E., & Humes, K. 2005. Dielectric loss and calibration of the hydra probe soil water sensor. Vadose Zone Journal, 4(4), 1070-1079. doi: 10.2136/vzj2004.0148

Seyfried, M. S., & Murdock, M. D. 2004. Measurement of soil water content with a 50-MHz soil dielectric sensor. Soil Science Society of America Journal, 68(2), 394-403.

Shangguan, W., Dai, Y. J., Duan, Q. Y., Liu, B. Y., & Yuan, H. 2014. A global soil data set for earth system modeling. Journal of Advances in Modeling Earth Systems, 6(1), 249-263. doi: 10.1002/2013ms000293

Singh, H. V., & Thompson, A. M. 2016. Effect of antecedent soil moisture content on soil critical shear stress in agricultural watersheds. Geoderma, 262, 165-173. doi: 10.1016/j.geoderma.2015.08.011

Temimi, M., Leconte, R., Chaouch, N., Sukumal, P., Khanbilvardi, R., & Brissette, F. 2010. A combination of remote sensing data and topographic attributes for the spatial and temporal monitoring of soil wetness. Journal of Hydrology, 388(1-2), 28-40. doi: 10.1016/j.jhydrol.2010.04.021

Trabucco, A., Zomer, R. J., Bossio, D. A., van Straaten, O., & Verchot, L. V. 2008. Climate change mitigation through afforestation/reforestation: A global analysis of hydrologic impacts with four case studies. Agriculture Ecosystems & Environment, 126(1-2), 81-97. doi: 10.1016/j.agee.2008.01.015

van der Velde, R., Su, Z., Ek, M., Rodell, M., & Ma, Y. 2009. Influence of thermodynamic soil and vegetation parameterizations on the simulation of soil temperature states and surface fluxes by the Noah LSM over a Tibetan plateau site. Hydrology and Earth System Sciences, 13(6), 759-777.

Verhoest, N. E. C., van den Berg, M. J., Martens, B., Lievens, H., Wood, E. F., Pan, M., et al. 2015. Copula-Based Downscaling of Coarse-Scale Soil Moisture Observations With Implicit Bias Correction. Ieee Transactions on Geoscience and Remote Sensing, 53(6), 3507-3521. doi: 10.1109/tgrs.2014.2378913

Vero, S. E., Antille, D. L., Lalor, S. T. J., & Holden, N. M. 2014. Field evaluation of soil moisture deficit thresholds for limits to trafficability with slurry spreading equipment on grassland. Soil Use and Management, 30(1), 69-77. doi: 10.1111/sum.12093

Viterbo, P., & Beljaars, A. C. M. 1995. An improved land surface parameterization scheme in the ECMWF model and its validation. Journal of Climate, 8(11), 2716-2748. doi: 10.1175/1520-0442(1995)008<2716:ailsps>2.0.co;2

Walker, J. P., Willgoose, G. R., & Kalma, J. D. 2001. The Nerrigundah data set: Soil moisture patterns, soil characteristics, and hydrological flux measurements. Water Resources Research, 37(11), 2653-2658. doi: 10.1029/2001wr000545

Walter, I. A., Allen, R. G., Elliott, R., Jensen, M. E., Itenfisu, D., Mecham, B., et al. 2000. ASCE's standardized reference evapotranspiration equation. Amer Soc Agricultural & Biological Engineers St Joseph.

Werbylo, K. L., & Niemann, J. D. 2014. Evaluation of sampling techniques to characterize topographically-dependent variability for soil moisture downscaling. Journal of Hydrology, 516, 304-316. doi: 10.1016/j.jhydrol.2014.01.030

Western, A. W., & Grayson, R. B. 1998. The Tarrawarra data set: Soil moisture patterns, soil characteristics, and hydrological flux measurements. Water Resources Research, 34(10), 2765-2768. doi: 10.1029/98wr01833

Western, A. W., Grayson, R. B., Bloschl, G., Willgoose, G. R., & McMahon, T. A. 1999. Observed spatial organization of soil moisture and its relation to terrain indices. Water Resources Research, 35(3), 797-810. doi: 10.1029/1998wr900065

Williams, M., Richardson, A. D., Reichstein, M., Stoy, P. C., Peylin, P., Verbeeck, H., et al. 2009. Improving land surface models with FLUXNET data. Biogeosciences, 6(7), 1341-1359.

Wilson, D. J., Western, A. W., & Grayson, R. B. 2005. A terrain and data-based method for generating the spatial distribution of soil moisture. Advances in Water Resources, 28(1), 43-54. doi: 10.1016/j.advwatres.2004.09.007

Wilson, D. J., Western, A. W., Grayson, R. B., Berg, A. A., Lear, M. S., Rodell, M., et al. 2003. Spatial distribution of soil moisture over 6 and 30 cm depth, Mahurangi river catchment, New Zealand. Journal of Hydrology, 276(1-4), 254-274. doi: 10.1016/s0022-1694(03)00060-x

Yang, K., Qin, J., Zhao, L., Chen, Y. Y., Tang, W. J., Han, M. L., et al. 2013. A multi-scale soil moisture and temperature regularly automatic monitoring network aim at multi-satellite data validation in Tibet Plateau. Bulletin of the American Meteorological Society, 94(12), 1907-1916. doi: 10.1175/bams-d-12-00203.1

Yuge, K., Anan, M., Hamagami, K., & Hamada, K. 2016. Evaluation of the effect of soil moisture condition on crop bioelectrical potential. In XXIX International Horticultural Congress on Horticulture: Sustaining Lives, Livelihoods and Landscapes Vol. 1112, pp. 255-260.

Zak, S. K., & Beven, K. J. 1999. Equifinality, sensitivity and predictive uncertainty in the estimation of critical loads. Science of the Total Environment, 236(1-3), 191-214. doi: 10.1016/s0048-9697(99)00282-x

Zhang, X. Q., Ren, Y., Yin, Z. Y., Lin, Z. Y., & Zheng, D. 2009. Spatial and temporal variation patterns of reference evapotranspiration across the Qinghai-Tibetan Plateau during 1971-2004. Journal of Geophysical Research-Atmospheres, 114. doi: 10.1029/2009jd011753

# APPENDIX

The following symbols are used in this paper:

| Category | Description | Symbol |
|---|---|---|
| Model variables | Soil moisture | $\theta$ |
| | Infiltration | $F$ |
| | Deep drainage | $G$ |
| | Lateral flow | $L$ |
| | Evapotranspiration | $E$ |
| | Precipitation rate | $F_{\max}$ |
| | Fractional vegetation cover | $V$ |
| | Topographic curvature | $\kappa$ |
| | Length of the DEM grid cell | $c$ |
| | Topographic slope | $S$ |
| | Spatial average elevation | $\overline{Z}$ |
| | Local elevation | $Z$ |
| | Potential solar radiation | $I_p$ |
| | Contributing area | $A$ |
| | Spatial average soil moisture | $\overline{\theta}$ |
| | Deep drainage index | DDI |
| | Lateral flow index | LFI |
| | Radiative ET index | REI |
| | Aerodynamic ET index | AEI |
| Climate parameters | Coarse potential evapotranspiration | $\overline{E}_p$ |
| | PET elevation dependence | $\omega$ |
| | Priestley-Taylor coefficient | $\alpha$ |
| Soil parameters | Porosity | $\phi$ |
| | Vertical saturated hydraulic conductivity | $K_{s,v}$ |
| | Vertical pore disconnectedness | $\gamma_v$ |
| | Horizontal pore disconnectedness | $\gamma_h$ |
| | Soil depth where topographic curvature is zero | $\delta_0$ |
| | Minimum topographic curvature with soil | $\kappa_{\min}$ |
| | Anisotropy of saturated hydraulic conductivity | $\iota$ |
| | Relation of hydraulic to topographic gradient | $\varepsilon$ |
| Vegetation parameters | Interception efficiency | $\lambda$ |
| | Portion of transpiration from soil layer | $\eta$ |
| | Shading effect on soil evaporation | $\mu$ |
| | Aerodynamic ET exponent | $\beta_a$ |
| | Radiative ET exponent | $\beta_r$ |

# LIST OF ABBREVIATIONS

AMSR – Advanced Microwave Scanning Radiometer

ASCAT – Advanced Scatterometer

ASTER – Advanced Spaceborne Thermal Emission and Reflection Radiometer

CFSR – Climate Forecast System Reanalysis

CGIAR-CSI – Consultative Group for International Agriculture Research Consortium for Spatial Information

CLM – Community Land Model

DEM – digital elevation model

ECMWF – European Centre for Medium-Range Weather Forecasts

EMT+VS – Equilibrium Moisture from Topography, Vegetation, and Soil

ET – evapotranspiration

GHCN – Global Historical Climate Network

GLUE – Generalized Likelihood Uncertainty Estimation

HydroSHEDS – Hydrological data and maps based on SHuttle Elevation Derivatives at multiple Scales

IGBP – International Geosphere Biosphere Programme

ISRIC-WISE – International Soil Reference and Information Centre World Inventory of Soil property Estimates.

IQR – interquartile range

MODIS – MODerate resolution Imaging Spectroradiometer

NCEI – National Centers for Environmental Information

NCEP – National Centers for Environmental Prediction

NSCE – Nash Sutcliffe Coefficient of Efficiency

NOAA – National Oceanic and Atmospheric Administration

PSRI – potential solar radiation index

RMSE – root mean square error

SAVI – soil adjusted vegetation index

SiB – simple biosphere

SMAP – Soil Moisture Active Passive

SMOS – Soil Moisture Ocean Salinity

SRTM – Shuttle Radar Topography Mission

TOPLATS – TOPMODEL-Based Land-Atmosphere Transfer Scheme

VIC – Variable Infiltration Capacity